

mRNA Openers and Closers: Modulating AU-Rich Element-Controlled mRNA Stability by a Molecular Switch in mRNA Secondary Structure

Nicole-Claudia Meisner,^[a] Jörg Hackermüller,^[b, c] Volker Uhl,^[a] András Aszódi,^[b] Markus Jaritz,^[b] and Manfred Auer^{*[a]}

Approximately 3000 genes are regulated in a time-, tissue-, and stimulus-dependent manner by degradation or stabilization of their mRNAs. The process is mediated by interaction of AU-rich elements (AREs) in the mRNA's 3'-untranslated regions with trans-acting factors. AU-rich element-controlled genes of fundamentally different functional relevance depend for their activation on one positive regulator, HuR. Here we present a methodology to exploit this central regulatory process for specific manipulation of AU-rich element-controlled gene expression at the mRNA level. With a combination of single-molecule spectroscopy, computational biology, and molecular and cellular biochemistry, we show that mRNA recognition by HuR is dependent on the presentation of the sequence motif NNUUNUUU in single-stranded conformation. The presentation of the HuR binding site in the mRNA secondary structure appears to act analogously to a regulatory on/off switch that specifically controls HuR access to mRNAs in cis. Based on this finding we present a methodology for manipulating ARE mRNA levels by actuating this conformational switch specifically in a target mRNA. Computationally designed oligonucleotides (openers) enhance the NNUUNUUU ac-

cessibility by rearranging the mRNA conformation. Thereby they increase in vitro and endogenous HuR-mRNA complex formation which leads to specific mRNA stabilization (as demonstrated for TNF α and IL-2, respectively). Induced HuR binding both inside and outside the AU-rich element promotes functional IL-2 mRNA stabilization. This opener-induced mRNA stabilization mimics the endogenous IL-2 response to CD28 stimulation in human primary T-cells. We therefore propose that controlled modulation of the AU-rich element conformation by mRNA openers or closers allows message stabilization or destabilization in cis to be specifically triggered. The described methodology might provide a means for studying distinct pathways in a complex cellular network at the node of mRNA stability control. It allows ARE gene expression to be potentially silenced or boosted. This will be of particular value for drug-target validation, allowing the diseased phenotype to ameliorate or deteriorate. Finally, the mRNA openers provide a rational starting point for target-specific mRNA stability assays to screen for low-molecular-weight compounds acting as inhibitors or activators of an mRNA structure rearrangement.

Introduction

Control of mRNA stability represents an essential regulatory level in eukaryotic gene expression. It ensures tight time-dependent regulation, which is of particular relevance for the coordinated expression of early response genes (ERGs). The presence of AU-rich elements (AREs) in the 3'-untranslated regions (UTRs) of messenger RNAs mediates their rapid degradation or stabilization. AREs exert their function by specific interaction with trans-acting factors. Among the at least 21 ARE-binding proteins identified so far, a positive regulatory effect has been attributed only to HuR (ELAVL1, RefSeq accession: NP_001410) and its neuronal homologues HuB, HuC, and HuD.^[1,2]

Up to 3000 potentially ARE-regulated genes have been proposed recently.^[3] Highly tissue- and stimulus-specific upregulation of individual messengers by HuR was shown for VEGF in response to hypoxia,^[4] for TNF α in response to LPS or proinflammatory cytokine stimulation,^[5] for p21^[6] and p53^[7] after UV irradiation, for nitric oxide synthase II upon cytokine stimulation,^[8] for cyclins A and B1 in cell proliferation,^[9] or for c-fos during G₀ to G₁ transition in NIH3T3 cells.^[10]

HuR appears to be a central node in the network of regulatory processes controlling functionally diverse ARE genes. A

tool that exploits the function of HuR to specifically up- or downregulate genes at the mRNA level will be equally attractive in systems biology and drug discovery.

We characterized the molecular mechanisms of HuR ARE recognition in vitro as well as in cellular systems by a combination of computational biology and quantitative confocal fluorescence fluctuation analysis at single-molecule resolution. The

[a] Mag. N.-C. Meisner,⁺ Dr. V. Uhl, Univ. Doz. Dr. M. Auer
Novartis Institutes for Biomedical Research Vienna
Discovery Technologies, Innovative Screening Technologies
Brunnerstraße 59, 1235 Vienna (Austria)
Fax: (+43) 186-634-593
E-mail: manfred.auer@pharma.novartis.com

[b] Mag. J. Hackermüller,⁺ Dr. A. Aszódi, Dr. M. Jaritz
Novartis Institutes for Biomedical Research Vienna
Informatics and Knowledge Management at NIBR, In Silico Sciences
Brunnerstraße 59, 1235 Vienna (Austria)

[c] Mag. J. Hackermüller⁺
University of Vienna
Institute for Theoretical Chemistry and Molecular Structural Biology
Währingerstraße 17, 1090 Vienna (Austria)

[*] These authors contributed equally to this work

identification of a secondary-structure dependence of HuR-mRNA recognition led us to the development of an algorithm for the rational design of mRNA *openers* or *closers*. These oligonucleotides manipulate ARE mRNA levels by inducing a conformational rearrangement in the mRNA. We propose the use of these openers/closers as a novel tool for the manipulation of mRNA stability, potentially allowing up to 3000 functionally different ARE genes to be boosted or silenced. Additionally, this methodology now provides a new concept in drug-discovery research: targeting mRNA regulation through specific manipulation of mRNA secondary structure in cis.

Results

NNUUNUUU is the HuR binding site

Exploiting the HuR ARE interaction for gene manipulation requires a detailed understanding of this molecular recognition. To date, neither the mechanism nor the RNA-sequence and structural prerequisites determining the recognition are clear. For a quantitative analysis of HuR RNA complexation, we used confocal fluorescence fluctuation analysis (2D fluorescence intensity distribution analysis or 2D-FIDA anisotropy^[11]). The method allows affinities to be determined in homogeneous solution, based on the measurement of true particle concentrations. It is particularly advantageous to conventional methods for measuring interactions between species of low solubility, high affinity, or variable stoichiometry. By using the IMPACTTM-CN purification strategy (New England Biolabs), full-length HuR was obtained in soluble form as native protein without a hydrophilic fusion tag. HuR bound to its native ARE target sequences with a high variation in affinities, with K_d s ranging from 130 pM to 13.6 nM (Table 1, exemplary binding curves in Figure 1).

Resolving the mechanistic reason for the 100-fold differences in dissociation constants might potentially enable us to actively modulate HuR-mRNA associations. The first step in this direction was a precise definition of the unresolved HuR binding site. In a recent study, De Silanes et al.^[12] observed that a short stem-loop without sequence constraints other than one uracil position is predictive for HuR targets. While it will be interesting to see whether this stem-loop motif contains binding sites for proteins associated with the HuR pathway, there is accumulating knowledge on the general RNA sequence preferences of HuR in the literature: essentially, multiple (AUUUA) repeats (e.g., ref. [13]) and U-rich stretches (e.g., ref. [14]) are known to be bound by HuR with high affinity. Additionally, a consensus binding motif of eight nucleotides (N-U/C-U-N-N-U/C-U-U/C) was deduced for the close homologue HuD_{1,2} from two X-ray structures of cocrystals with 11-mer RNAs.^[15] In contrast to the ARE core elements AUUUA and UUAUUUAUU,^[16] the presence or absence of this motif within the tested RNA sequences was consistent with our observed binding or nonbinding of HuR. However, no binding of HuR to 8-mer N-U/C-U-N-N-U/C-U-U/C variants (U₈ as well as AUUAAUUU, CUUCCUUU, GUUGGUUU) was observed experimentally. In previous experiments, we had found that HuR binds to U₃₀ with high affinity. We therefore

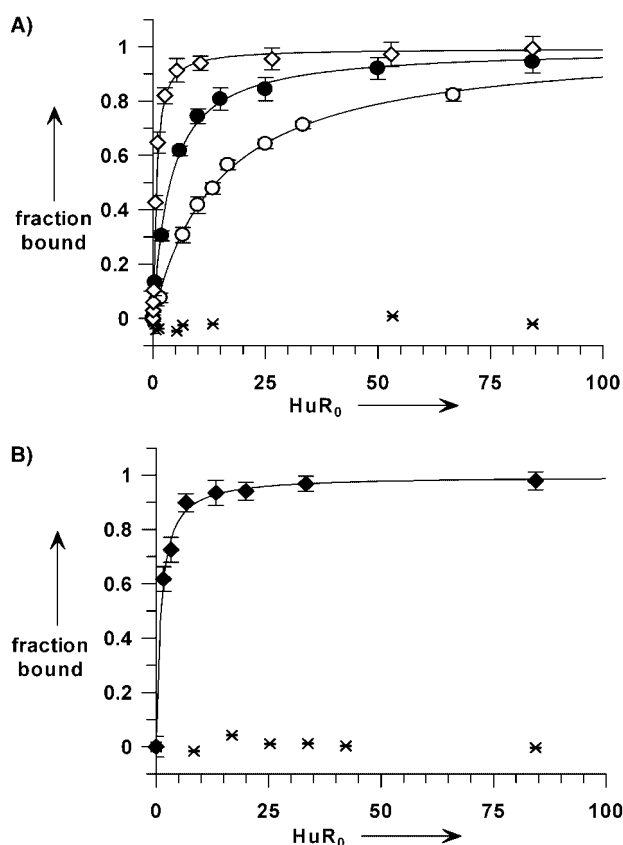


Figure 1. HuR-ARE interaction monitored with 2D-FIDA. Exemplary binding curves from anisotropy measurements with 2D-FIDA for monitoring HuR binding to TMR-labeled ARE RNAs (A) and 9-mer RNAs (B). For illustration, the anisotropy data were converted to the fraction of HuR-bound RNA according to $\text{fraction bound} = (r - r_{\text{min}}) / [(r - r_{\text{min}}) + Q(r_{\text{max}} - r)]$, with r_{min} : anisotropy of free RNA, r_{max} : anisotropy of HuR RNA complex, r : anisotropy of the RNA-HuR complex equilibrium at the given HuR_0 and RNA_0 concentrations; Q : quenching. The apparent dissociation constant $K_{d,\text{app}}$ was determined by nonlinear curve fitting of the anisotropy data as described in the Experimental Section. HuR binds to its target AREs with 100-fold different affinities. A) \diamond TNF α ARE (Figure 3, (6); r_{min} : 0.110 ± 0.003 , r_{max} : 0.2133 ± 0.003), \bullet IL-4 ARE (Figure 3, (4); r_{min} : 0.162 ± 0.004 , r_{max} : 0.278 ± 0.003), \circ Cox-2 ARE (Figure 3, (1), r_{min} : 0.162 ± 0.001 , r_{max} : 0.248 ± 0.004), \times (AUUU)₂A. B) \blacklozenge AAUUUAUUU (Figure 2, (9); r_{min} : 0.062 ± 0.001 , r_{max} : 0.106 ± 0.001), \times UUAUUUAUU (Figure 2, (4c)). All ARE sequences and K_d values are specified in Table 1 and Figure 2.

determined the minimal required length of oligoU for HuR binding. Remarkably, a one-nucleotide elongation from U₈ to U₉ was sufficient for high-affinity binding of HuR ($K_d = 0.97 \pm 0.19$ nM). Hence, HuR requires a minimum of nine nucleotides for recognition. As detailed in Figure 2, we deduced that the HuR binding site is the 9-mer N-N-U-U-N-N-U-U-U in a series of binding experiments with strategically designed fragments.

This HuR binding motif is further supported by an HuR homology model (data not shown) based on the structures of HuD (1FXL,1G2E)^[15] and Sxl (1B7F).^[17] It is present in all validated HuR target mRNAs currently described in the literature (see Table 2) and in 98.7% of all 896 sequences in ARED 1.0, a database of in silico-identified ARE mRNAs^[3] (100% in clusters I-IV, 97.9% in cluster V). Additionally, the frequency of NNUUN-NUUU-containing sequences is significantly higher in the set of

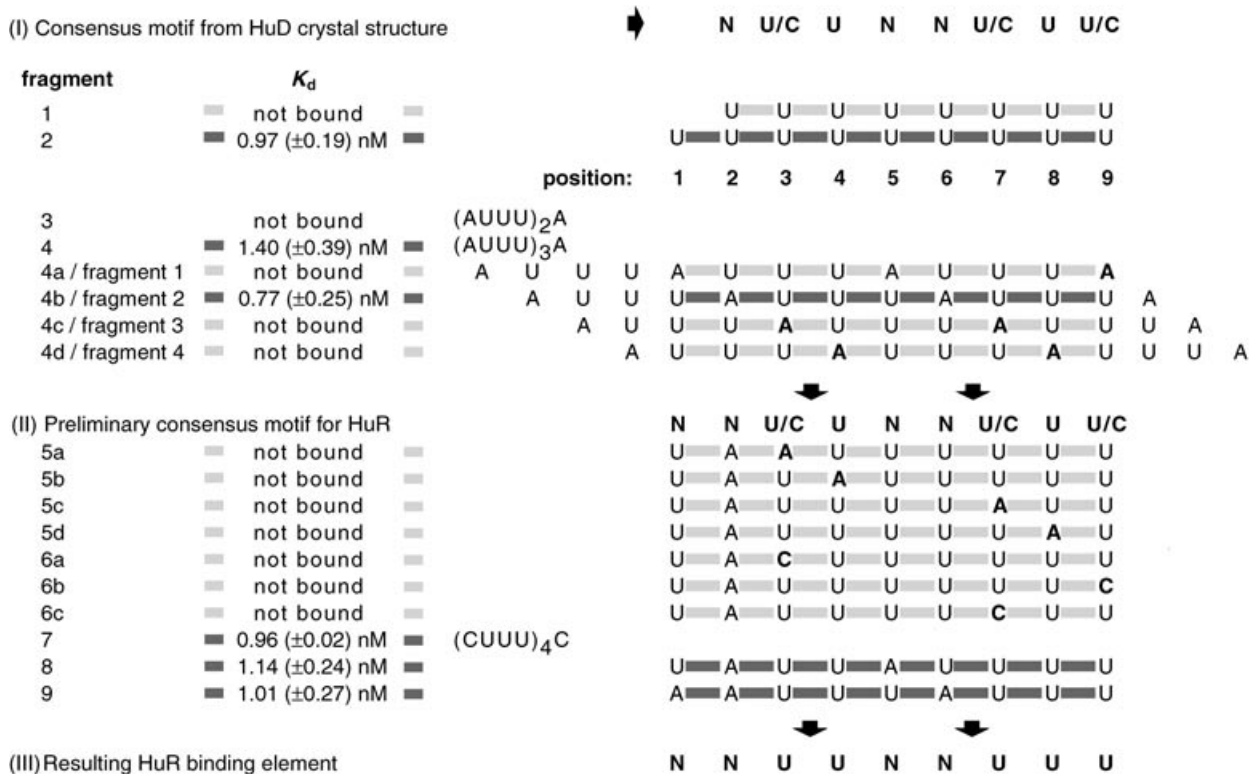


Figure 2. Experimental deduction of the HuR binding site. The experimentally determined affinity (K_d) of full-length HuR to the individual synthetic RNA fragments (nucleotides connected with gray bars) is shown. The proposed and tested consensus motifs are given in bold. While the simplest variant of the previously proposed consensus motif for HuD, U_9 (fragment 1) was not recognized by HuR,^[116] an elongation by one nucleotide to U_9 (fragment 2) was necessary and sufficient for high-affinity binding. An influence of the fluorescent dye was excluded by competition experiments with unlabeled RNA fragments (data not shown). A 3'-terminally elongated HuD motif (9-mer fragment 3) was not bound by HuR.^[116] However the high-affinity binding to fragment 4 indicates that non-U nucleotides are tolerated within the HuR binding motif, but only at certain positions. Knowing that nine nucleotides are sufficient for recognition, one finds four different 9-mer frames within $(AUUU)_3A$. Among the four corresponding fragments (4a–4d) the exclusive recognition of fragment 4b demonstrates that HuR binds to frame 2 within $(AUUU)_3A$. This frame is consistent with the HuD motif, but 5'-terminally elongated by one uracil residue; this suggests the preliminary binding motif N-N-U/C-U-N-N-U/C-U-U/C. Fragments 5a–5d, 6a–6c, 7, 8, and 9 served to test the tolerance for non-U (exemplified by A) and C, respectively, at the depicted (bold) positions. In consequence, we propose that the HuR sequence binding motif is N-N-U-U-N-N-U-U-U. This interaction appears to follow an “all-or-nothing”^[116] mechanism. While sequences with single mismatches are not recognized,^[116] sequences fulfilling this motif are bound with high affinity and an invariable K_d , $K_{d, \text{fund}}$ of 0.96 ± 0.48 nM.

(All concentrations represent equilibrium concentrations). Accordingly, $K_{d, \text{app}}$ is a function of p and can be expressed as:

$$K_{d, \text{app}} = K_{d, \text{fund}} \cdot \frac{1}{p} \quad (3)$$

We express this *accessibility* p as the thermodynamic probability of structures that contain at least one NNUUNUUU in single-stranded conformation within the secondary structure ensemble of an RNA sequence, henceforth also denoted as $p(ssNNUUNUUU)$. For NNUUNUUU-containing fragments that are too short to form stable secondary structures, $p=1$. p becomes <1 for an ensemble of an ARE sequence containing NNUUNUUU hidden in the secondary structure. This leads to an increase in the experimentally observed K_d , $K_{d, \text{app}}$ compared to $K_{d, \text{fund}}$. As detailed in Figure 3, experimentally determined $K_{d, \text{app}}$ values show the anticipated reciprocal dependence on the calculated accessibility, p . Following a statistical test described in ref. [20], $K_{d, \text{app}}$ is shown to be significantly correlated with $1/p$ at the 99% level. For the relatively short RNA sequen-

ces tested, any trapping in local secondary-structure optima was neglected, as they typically have a rather simply structured free-energy landscape. Such effects might rather play a role for longer sequences like UTRs or full-length mRNAs. In such a case, we should observe a strong deviation from the predicted dependence of $K_{d, \text{app}}$ on the accessibility p . However, the correlation even holds for HuR binding affinities to AREs within the tested full-length 3'UTRs (Figure 3, fragments 14 and 15). To corroborate our motif-accessibility model, we followed a strategy of sequence elongation starting from an exemplary NNUUNUUU core. By synthesizing up- and downstream elongated variants of the natural TNF α -ARE, we modulated the secondary structure. Thereby the accessibility of NNUUNUUU within the secondary structure was reduced without altering the core ARE sequence. The experimentally measured affinities of the elongated ARE fragments were *decreased*, and in good agreement with the predicted values based on the accessibility $p(ssNNUUNUUU)$ as compared to the core ARE fragment (Figure 3, fragments 7 and 8; Figure 4, TNF α_{42} and TNF α_{45}). Also a strategically designed variant of given theoretical acces-

Table 2. NNUUNUUU is present in validated mammalian HuR targets.^[a]

Gene symbol	Gene name, alternative names	Sequence ID	Ref.	ARED2.0	Contains NNUUN-UUUU
Cytokines, chemokines, growth factors					
BMP6	bone morphogenetic protein 6	NM_001718	[68]	V	x
CCL11	chemokine (C-C motif) ligand 11, eotaxin	NM_002986	[69]		x
CSF2	colony stimulating factor 2, GM-CSF	NM_000758	[22,70–72]	I	x
FSHB	follicle stimulating hormone β	AH003599	[73]		x
IL1b	interleukin 1 beta	NM_000576		II	x
IL2	interleukin 2	NM_000586	[74,26,72]	III	x
IL3	interleukin 3	NM_000588	[21,75,76]	V	x
IL4	interleukin 4	NM_000589		III	x
IL6	interleukin 6	NM_000600	[68]	IV	x
IL8	interleukin 8	NM_000584	[68,77,78]	II	x
MYOD1	myogenic factor 3	NM_002478	[79,80]		x
MYOG	myogenin	NM_002479	[79,80]		x
NF1	neurofibromin 1	NM_000267	[81]		x
PITX2	paired-like homeodomain transcription factor 2	NM_000325	[82]		x
TNF α	tumor necrosis factor α	NM_000594	[5,30,83–85]	III	x
VEGF	vascular endothelial growth factor	NM_003376	[86–89]	IV	x
Tumor suppressor genes, proto-oncogenes, cell-cycle regulators					
CCNA2	cyclin A	NM_001237	[9,90]		x
CCNB1	cyclin B1	NM_031966	[9,90]		x
CCND1	cyclin D1	NM_053056	[9,82,90]	V	x
CCND2	cyclin D2	NM_001759	[82]		x
CD83	CD83 antigen	NM_004233	[91]		x
CDKN1A	cyclin-dependent kinase inhibitor 1A, p21, Cip1	NM_000389	[6,79,92]		x
CDKN1B	cyclin-dependent kinase inhibitor 1B, p27,kip1	NM_004064	[28]		x
DEK	DEK oncogene	NM_003472	[93]		x
FOS	v-fos FBJ murine osteosarcoma viral oncogene homologue, c-fos	NM_005252	[10,75,94,95]	IV	x
HLF	hepatic leukemia factor	NM_002126	[93]		x
JUN	v-jun sarcoma virus 17 oncogene homologue (avian), c-jun	NM_002228	[82,94]		x
MYC	v-myc myelocytomatosis viral oncogene homologue, c-myc	NM_002467	[96,97]		x
MYCN	v-myc myelocytomatosis viral related oncogene, neuroblastoma derived, n-myc	NM_005378	[75,98]		x
TP53	tumor protein p53	NM_000546	[7,99]		x
Enzymes					
HDAC2	histone deacetylase 2	NM_001527	[93]		x
MMP9	matrix metalloproteinase 9	NM_004994	[100,101]		x
NDUFB6	NADH dehydrogenase (ubiquinone) 1 β subcomplex	NM_002493	[93]		x
NOS2A	nitric oxide synthase 2A	NM_000625	[8]		x
PLAU	urokinase plasminogen activator	NM_002658	[23]	IV	x
PTGS2	prostaglandin-endoperoxide synthase 2, COX2	NM_000963	[68,89,102–105]	III	x
SERPINB2	serine (or cysteine) proteinase inhibitor, PAI-2	NM_002575	[106]	V	x
UBE2N	ubiquitin-conjugating enzyme E2N	NM_003348	[93]		x
Receptors, membrane proteins					
ADRB1	β 1-adrenergic receptor	NM_000684, U29690	[107,108]		x
ADRB2	β 2 adrenergic receptor	NM_000024	[107,108]		x
AR	androgen receptor	NM_000044	[14,109]		x
CALCR	calcitonin receptor	NM_001742	[110]		x
CDH2	cadherin 2, type 1, N-cadherin	NM_001792	[93]		x
GAP43	growth associated protein 43	NM_002045	[111]		x
SLC2A1	solute carrier family 2 member 1, GLUT1	NM_006516	[112]		x
PLAUR	urokinase plasminogen activator receptor	NM_002659	[23]	IV	x
SLC5A1	solute carrier family 5, SGLT1	NM_000343	[113]		x
TNFSF5	tumor necrosis factor (ligand) superfamily, member 5, CD154	NM_000074	[114]	IV	x
Miscellaneous					
ACTG1	actin, γ 1	NM_001614	[93]		x
CTNNB1	catenin (cadherin-associated protein), beta 1	NM_001904	[12]		x
MARCKS	myristoylated alanine-rich protein kinase C substrate	NM_002356	[25]		x
MTA1	metastasis associated 1	NM_004689	[93]		x
PITX2	paired-like homeodomain transcription factor 2	NM_000325	[82]		x
SLC7A1	cationic amino acid transporter, CAT-1	NM_003045	[115]		x

[a] The presence of NNUUNUUU in human orthologous mRNAs of validated mammalian HuR targets has been tested. ARED2.0^[45] cluster numbers are specified for sequences contained in this database. Binding of HuR to mRNAs without a reference in the table has been shown in this study for the first time (Table 1). Renin mRNA, for which HuR associated stability control has been reported recently,^[67] contains the motif but with a single U to C mismatch.

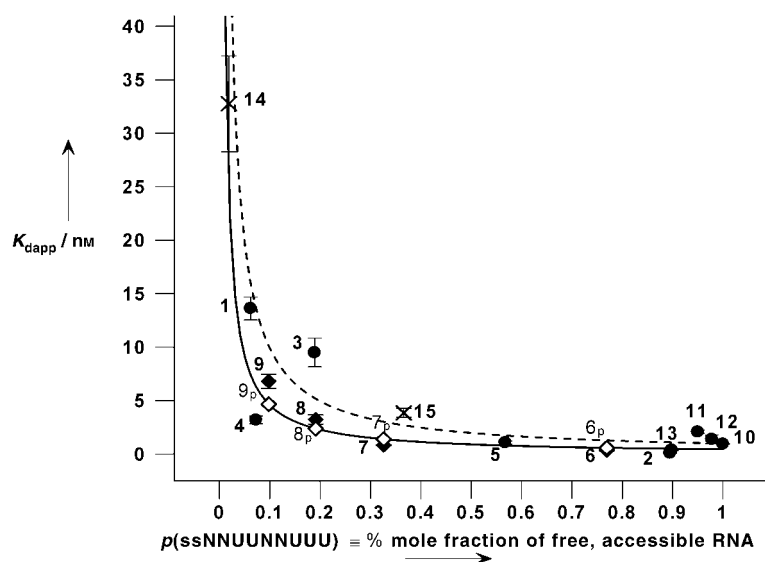


Figure 3. Correlation between accessibility of NNUUNUUU within AREs and observed K_d ($K_{d,app}$). Experimentally determined affinities of HuR to the AREs of Cox-2 (1), IL-1 β (2), IL-2 (3), IL-4 (4), IL-8 (5), to (AUUU) $_3$ A (10), (AUUU) $_2$ A (11), (AUUU) $_3$ A (12), (CUUU) $_2$ C (13) (\bullet), to the 3'UTRs of IL-2 and TNF α (14 and 15, \times), and to the ARE of TNF α (6) as well as the strategically designed variants TNF α_{42} (7), TNF α_{45} (8), and TNF α_{mut} (9) (\blacklozenge) and their predicted values (\diamond) are plotted against the corresponding accessibilities of the HuR binding motif p(ssNNUUNUUU), which is the thermodynamic probability of structures in the ensemble which contain NNUUNUUU in a single-stranded conformation. As shown in Figure 2, HuR binds to NNUUNUUU elements with an almost invariable K_d , $K_{d,fund}$. The correlation between measured affinities $K_{d,app}$ and calculated accessibilities p follows the derived reciprocal dependence $K_{d,app} = K_{d,fund}/p$. The dotted line depicts the resulting graph for the approximation of $K_{d,fund}$ by the experimentally determined value of 0.96 ± 0.48 nM (Figure 2). The solid line depicts the graph obtained by nonlinear curve fitting of the data ($K_{d,app} = (0.49 \pm 0.09)/p$).

sibility showed the predicted apparent K_d in the binding experiments (Figure 3, fragment 9). These data provide strong evidence for the validity of the accessibility hypothesis. We conclude, that it is the ARE secondary structure that determines the effective concentration of the HuR binding motif and thereby the extent of HuR–mRNA complex formation.

ARE secondary structure as a molecular switch

The categoric-sequence and secondary-structure discrimination between binding of HuR to AREs with very high affinity and no detectable binding at all^[116] points to a regulatory switch in the binding-site presentation. To exploit such a switch, the secondary structure of endogenous mRNA needs to be specifically and actively modulated. We rationally designed short oligonucleotides (length arbitrarily set to 20 nt) as trans-acting secondary-structure modulators, henceforth denoted *openers* (*closers*). These reverse complementary openers (*closers*) were constructed to maximize (minimize) the HuR binding-site accessibility of their target mRNA upon hybridization (Figure 5). We performed opener predictions for IL-2 and TNF α (Figure 6). Remarkably, a significant accessibility change is restricted to “hotspots” within the mRNA, mainly located outside but in proximity to the HuR binding sites. At other positions, hybridization leaves the local ARE conformation almost unaffected. Three individual openers targeting either of the two HuR binding sites within the IL-2 3'UTR were selected for experimental verification (Op $_1$, Op $_2$, and Op $_3$ in Figure 6A, see also Table 3).

Designed secondary structure modulators enhance HuR–mRNA complexation in vitro and increase mRNA stability in cell lysates

We proceeded to provide the biochemical and cell biological proof of concept for the functionality of such a secondary-structure mediated regulatory on/off mechanism. The opener effect was initially validated in vitro. As measured in a 1D-FIDA assay, HuR binds to the IL-2 3'UTR (281 nt) with significantly higher affinity in the presence of any of the openers (Figure 7B). The HuR IL-2 3'UTR affinity increases with the concentration of added opener (Figure 7C). A neg-

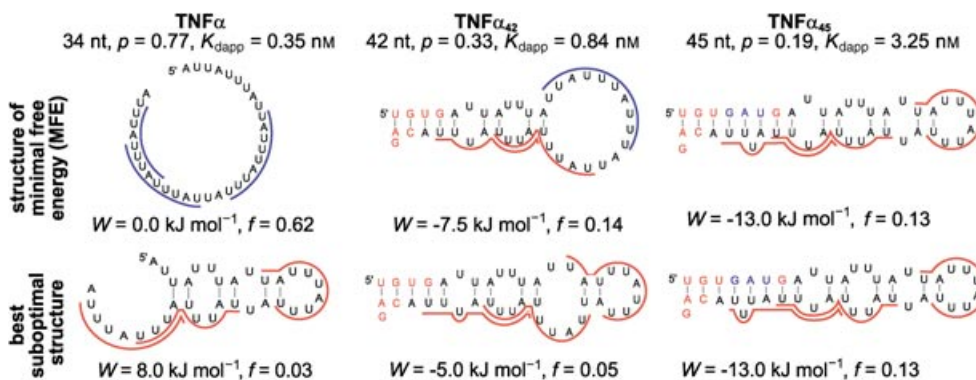


Figure 4. Secondary structure controls ARE recognition by HuR. The decrease in HuR affinity through ARE sequence elongation demonstrates the impact of binding site accessibility. Elongation of the 34-mer TNF α -ARE to the 42-mer and 45-mer variants TNF α_{42} and TNF α_{45} leads to a decrease in motif accessibility p which explains the observed decrease in affinity (increase in $K_{d,app}$). Red nucleotides: elongation of the wild-type (WT) sequence; blue nucleotides: elongation by additional AUG insertion. To illustrate the change in secondary structure, the minimum-free-energy conformation and the best suboptimal structure are shown for each sequence (W = free energy; f = frequency in the thermodynamic ensemble). Accessible (i.e. single-stranded) NNUUNUUU HuR binding sites are underlined in blue, inaccessible sites are underlined in red.

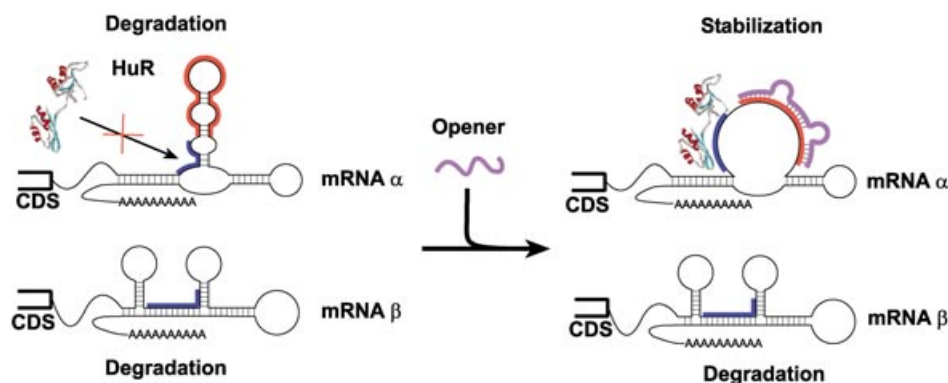


Figure 5. mRNA openers induce HuR access to mRNAs in cis. HuR binding to a messenger RNA is impaired by the inaccessibility of the binding site (marked in blue) within the mRNA secondary structure. Hybridization of the opener (depicted in violet) specifically provokes a conformational rearrangement in the target mRNA (mRNA α) to present the binding site in an accessible conformation. Any other HuR target mRNA present (exemplified by mRNA β) is protected from a malapropos activation by the inherent sequence specificity of the opener oligonucleotide. As a result, HuR is able to recognize the NNUUNUUU motif and stabilize the “opened” mRNA specifically in cis.

ative control was performed with an IL-2-specific 20-mer, which does not affect the accessibility $p(ssNNUUNUUU)$. Hybridization of this oligonucleotide to the IL-2 3'UTR does not influence the HuR–IL-2 3'UTR association (Figure 7 B, C).

To verify that the opener oligonucleotides also function in a more complex cellular environment, we quantified endogenous HuR IL-2 mRNA association in cell lysates as a model system. Cytoplasmic lysates of human peripheral blood mononuclear cells (PBMC) were treated with the opener oligonucleotides. This experimental approach allows defined concentrations to be achieved and prevents cellular stress responses induced by opener transfection. IL-2 mRNA HuR complexes were

co-immunoprecipitated in the presence or absence of the opener or negative control and HuR-bound IL-2 mRNA was quantified by real-time reverse-transcriptase polymerase chain reaction (RT-PCR). Unspecific immunoprecipitation was excluded by using a control antibody (goat IgG, data not shown). Indeed, both openers increase the level of HuR IL-2 mRNA association up to 6.5-fold in a concentration-dependent manner (Figure 8).

We finally examined the impact of the IL-2 openers in ARE-dependent mRNA degradation. In human PBMC lysates IL-2 mRNA decay—which we found to be Mg²⁺ dependent (data not shown)—was monitored in the presence and absence of either openers Op₁, Op₂ as well as Neg. Upon Mg²⁺ addition, the amount of remaining IL-2 mRNA was quantified over time by real-time RT-PCR. In absence of any opener, endogenous IL-2 mRNA is rapidly degraded ($t_{1/2} = 10.9 \pm 2.27$ min), while the mRNA of a non-ARE gene (elongation factor 1 α , EF1 α) is stable throughout the observation time of 70 min (Figure 9). The observed half-lives are comparable to previously described values;^[21] this indicates that such a degradation system (adopted from previously described protocols, such as refs. [22,23]) is a valid approximation of an in vivo situation. In the presence of opener Op₁ ($c = 10 \mu\text{M}$),

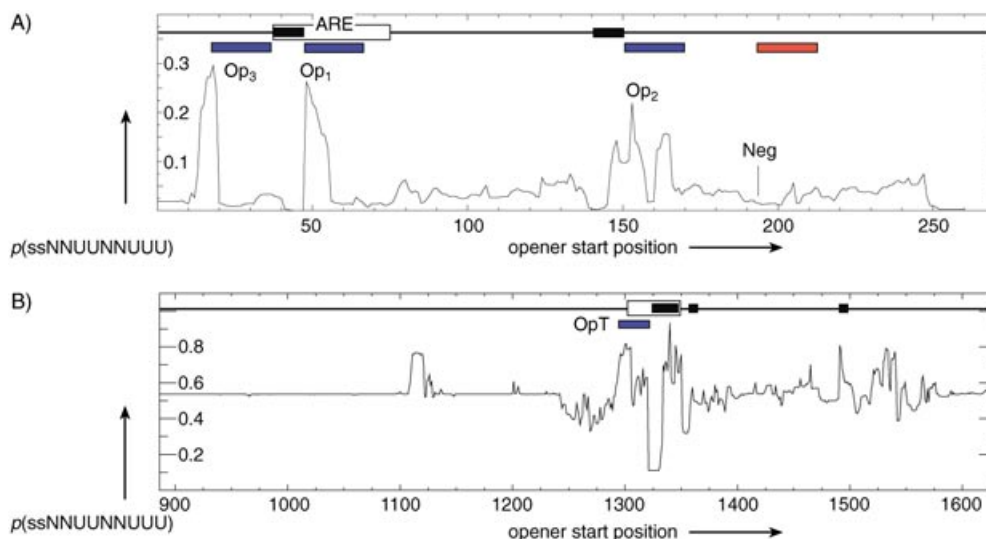


Figure 6. Design of opener oligonucleotides. The HuR binding-site accessibility $p(ssNNUUNUUU)$ in the IL-2 3'UTR (A) or TNF α mRNA (B) is shown in dependence of hybridization to a reverse complementary 20-mer oligonucleotide at a given start position within the respective target mRNA sequence (x-axis). The AU-rich element is indicated as a white box, NNUUNUUU HuR binding sites are marked by black boxes. Putative “opener” positions are identified based on a significant increase in the NNUUNUUU accessibility (local maxima), putative “closer” positions are marked by a predicted decrease in the accessibility (local minima). Interestingly, the opener positions are restricted to discrete “hotspots” in proximity to the HuR binding sites. The closers cluster mainly within the opener hotspot region. The locations of experimentally tested opener molecules Op_T (for TNF α) and Op₁, Op₂, Op₃ (for IL-2) are indicated in blue, negative control Neg (for IL-2) is shown in red (sequences specified in Table 3). Openers Op₁ and Op₃ target primarily the HuR binding site within the IL-2 ARE, Op₂ is directed to the second NNUUNUUU motif within the IL-2 3'UTR.

Table 3. Tested opener and negative-control oligonucleotides. ^[a]				
Target mRNA	RefSeq	Opener/Control	Positions	Sequence (5'→3')
IL-2	NM_000589	Op ₁	804–823	AATATAAAATTTAAATATTT
		Op ₂	909–928	TAGAGCCCTAGGGCTTACA
		Op ₃	920–939	TGAAACCATTTAGAGCCCC
		Neg	950–969	CATAATAATAAATATTTGG
TNF α	NM_000594	Op _r	1315–1334	ATCACAAGTGCAACATAAA

[a] Sequences of putative opener or negative control oligodeoxynucleotides selected for experimental testing are specified. The sequences are reverse complementary to the specified region in the target mRNA and given in 5' to 3' direction.

this degradation is completely halted over a period of 15 min (Figure 9A). At that time untreated IL-2 mRNA is already degraded to 79.9%. Also after 15 min incubation time, the decay is significantly slowed down. At 40 μ M concentration (Figure 9C), Op₁ blocks the degradation over the entire incubation time of 70 min. Op₂, which targets another HuR binding site, shows a similar stabilizing effect (Figure 9B and C). The degradation kinetics are not significantly changed by hybridization with the negative control oligonucleotide Neg ($t_{1/2} = 6.82 \pm 1.96$ min). To ensure that the opener-induced IL-2 mRNA stabilization is indeed a specific effect, we monitored the mRNA stability of other ARE-containing HuR targets. Neither TNF α nor IL-1 β mRNA decay is influenced by our IL-2 specific openers (Figure 10). Additionally, a TNF α opener (Op_r, Figure 6B) pro-

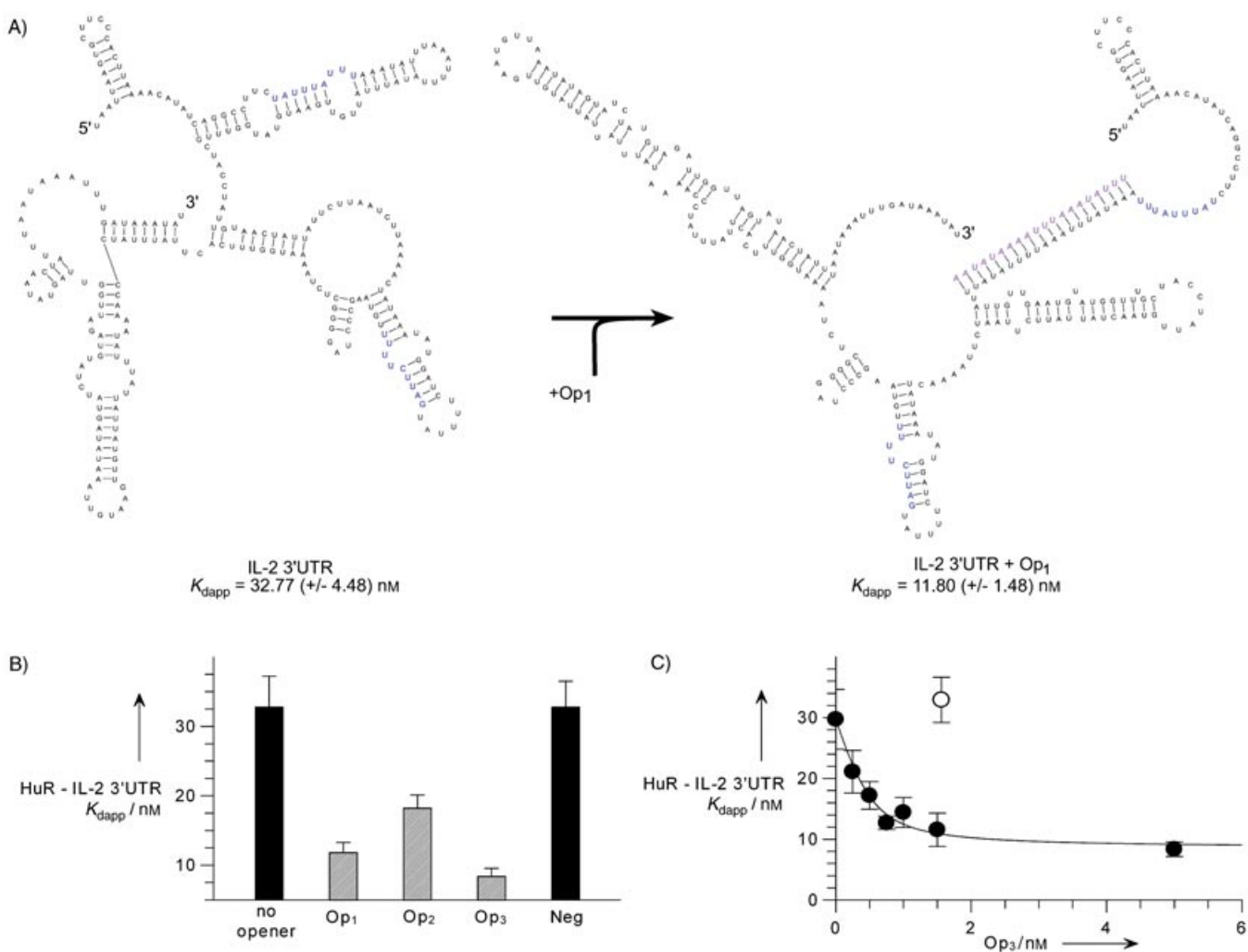


Figure 7. IL-2 openers increase HuR-IL-2 3'UTR complex formation in vitro. A) Predicted minimal free energy (MFE) secondary structure of the IL-2 3'UTR and of the IL-2 3'UTR hybridized to opener Op₁ (Op₁ represented in violet). NNUUNUUU elements are shown in blue. As exemplified and illustrated by the predicted MFE conformation of the complex, the opener shifts the equilibrium towards conformations with accessible (i.e. single-stranded) NNUUNUUU elements—following the model sketched in Figure 5. MFE secondary structures for 3'UTR–opener complexes were computed by using RNAcofold (available with the Vienna RNA package^[63]). B) All three tested IL-2-specific openers enhance the HuR association with the IL-2 3'UTR, reflected by a decrease in the apparent dissociation constant K_d (Op₁: $K_{dapp} = 11.80 \pm 1.48$ nM; Op₂: $K_{dapp} = 18.91 \pm 1.91$ nM, Op₃: $K_{dapp} = 8.38 \pm 1.18$ nM; without opener: $K_{dapp} = 32.77 \pm 4.48$ nM; IL-2 3'UTR at 0.5 nM; Op₁ and Op₃ at the concentration optimum of 1.56 and 5 nM, respectively; Op₂ at 25 nM). Hybridization of the negative-control oligonucleotide Neg to the IL-2 3'UTR leaves the interaction with HuR unaffected ($K_{dapp} = 32.77 \pm 3.72$ nM, Neg at 25 nM concentration). C) The affinity increase induced by opener hybridization shows a saturation curve with half-maximal saturation at an opener concentration of 0.38 nM (shown for Op₃, apparent affinity of Op₃ hybridization = 134 ± 54 μ M). The apparent affinity of HuR binding to the opened IL-2 3'UTR approaches a maximum at a K_d minimum of 8.57 ± 1.33 nM. (● Op₃, ○ Neg at 1.56 nM, IL-2 3'UTR is at 0.5 nM in all experiments).

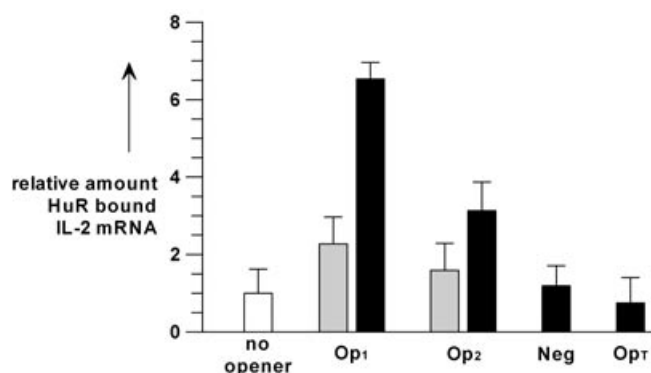


Figure 8. IL-2 mRNA openers increase endogenous HuR–IL2 mRNA association. HuR–mRNA complexes were co-immunoprecipitated from lysates of human PBMC without or after treatment with opener or negative-control oligonucleotides Op_1 , Op_2 , Neg, and Op_T . HuR-bound IL-2 mRNA was quantified by real-time RT-PCR. IL-2 mRNA amounts were normalized to the levels in untreated cells (white bar). Openers were added to $2.5 \mu\text{M}$ (gray bars) or $10 \mu\text{M}$ (black bars), negative controls Neg and Op_T to $10 \mu\text{M}$ concentration. Op_1 and Op_2 boost HuR–mRNA complexation to up to 6.5- or 3.1-fold higher levels, respectively.

motes TNF α mRNA stabilization in an equally specific manner (Figure 10). Furthermore, the opener-induced IL-2 mRNA stabilization is neutralized in the presence of an HuR specific antibody; this supports the HuR dependence of the opener action (Figure 11, opener Op_2). We conclude that mRNA openers provide a functional tool to manipulate HuR–mRNA complex formation and the associated mRNA half-life through a switch in mRNA conformation.

Discussion

Molecular mechanism of HuR ARE recognition

Previous studies on HuR–mRNA interactions in the literature had mapped HuR binding to mRNA subfragments containing AUUUA repeats or U-rich stretches (e.g. ref. [13,14]). Starting from the previously suggested HuD consensus motif (N-U/C-U-N-N-U/C-U-U/C^[15]) we identified the 9-mer N-N-U-U-N-N-U-U-U as the precise HuR binding site that so far had remained unrevealed in U-rich elements. The relevance of the NNUUNUUU motif is emphasized by its presence in all validated HuR target mRNAs currently described in the literature (Table 2) and its compliance with previous data on mapping HuR binding to mRNAs.^[24–27] That adenosines are not essential for the recognition by the “ARE binding” protein HuR is consistent with the previously noted existence of HuR targets that lack classical AREs.^[25,28] A conservation of adenosines in HuR binding sites is hence not associated with HuR recognition. Rather, it could be the result of an overlap with binding sites for negative regulators such as AUF-1 or TTP. Another evolutionary rationale for A's in AREs could be to interfere with the formation of a stable stack between U-rich stretches and the polyA tail as this would affect proper ARE and polyA function.

While the degenerate nature of the motif NNUUNUUU is consistent with the high number of ARE-controlled genes, the presence of the sequence motif alone does not provide an ex-

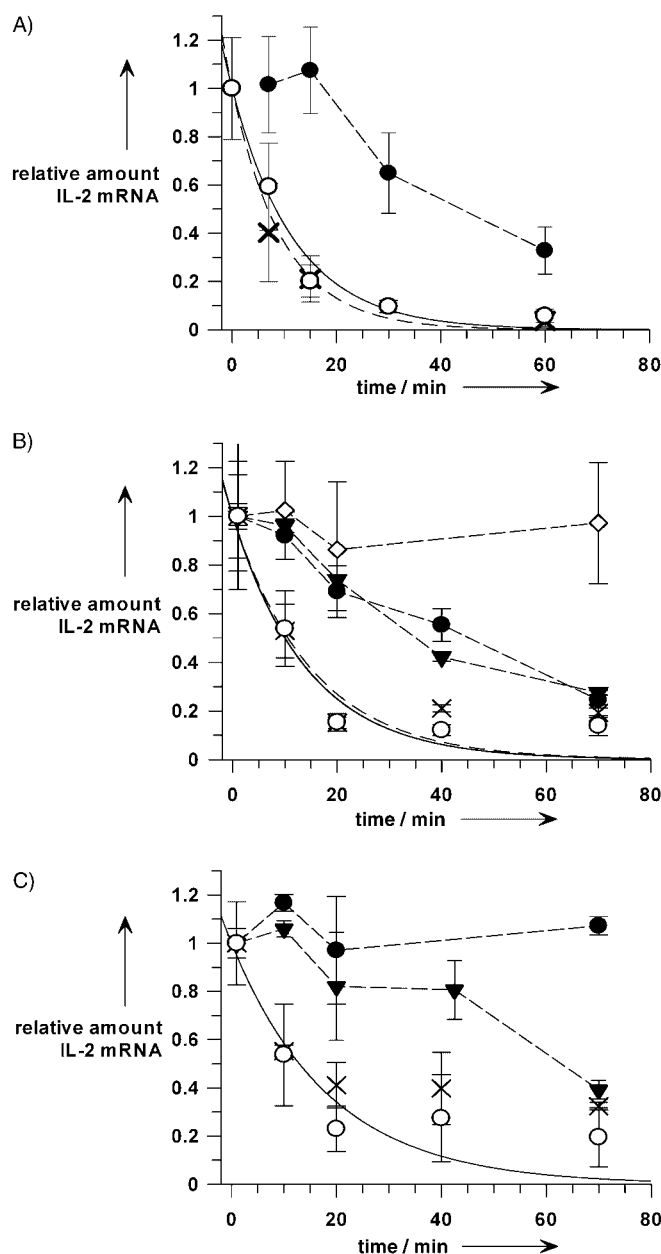


Figure 9. IL-2 mRNA openers inhibit IL-2 mRNA degradation. Degradation of endogenous IL-2 mRNA was monitored in human PBMC lysates. Upon the addition of Mg^{2+} ($t=0$ min), the amount of remaining IL-2 mRNA was quantified over time in the presence and absence of openers Op_1 , Op_2 or Neg at A) $10 \mu\text{M}$ (i.e. 2 fmol per cell), B) $25 \mu\text{M}$ (i.e. 5 fmol per cell), and C) $40 \mu\text{M}$ (i.e. 8 fmol per cell) by quantitative real-time RT-PCR. All data represent averages of at least three independent samples and were normalized to the levels at time point $t=0$ min. The data were fitted to a single exponential decay (— no opener, ---- Neg). IL-2 mRNA is rapidly degraded with a half-life of $t_{1/2} = 10.9 \pm 2.27$ min without any opener (\circ), as well as in presence of $10 \mu\text{M}$ negative control Neg (\times , $t_{1/2} = 6.82 \pm 1.96$ min). Addition of openers Op_1 (\bullet) or Op_2 (\blacktriangledown) promotes a transient IL-2 mRNA stabilization in a concentration-dependent manner. At $40 \mu\text{M}$, Op_1 blocks the degradation over the entire incubation time of 70 min. Op_2 shows a similar stabilizing effect, although it targets another HuR binding site (\blacktriangledown). EF-1 α , a non-ARE mRNA, remains stable over the entire observation time of 70 min (\diamond).

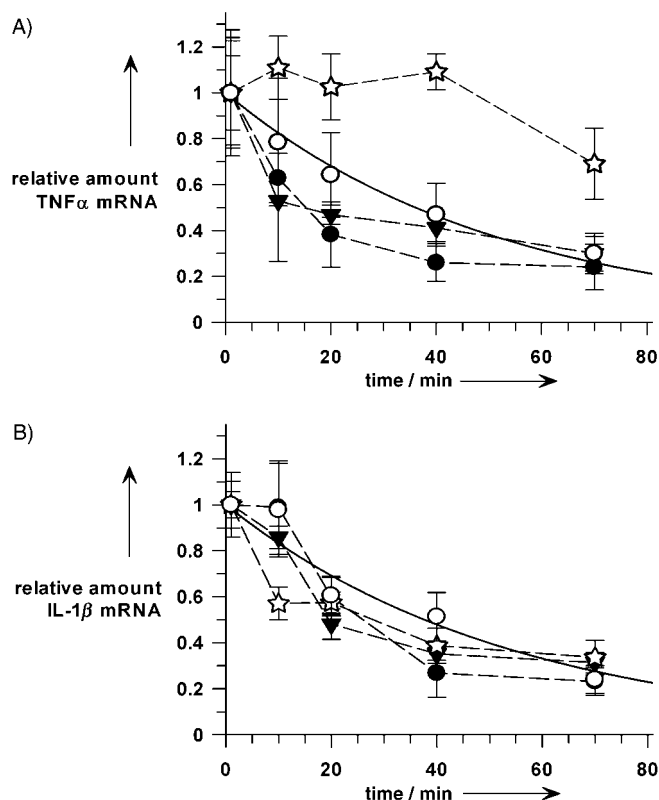


Figure 10. Opener oligonucleotides specifically promote ARE mRNA stabilization. The specificity of the opener-induced mRNA stabilization was tested by monitoring the IL-2 openers' effect on the decay of other ARE-containing cytokine mRNAs (TNF- α (A) and IL-1 β (B)). TNF- α and IL-1 β mRNA degradation is characterized by a half-life of $t_{1/2} = 36.0 \pm 2.2$ min (\circ , A) and $t_{1/2} = 37.6 \pm 5.6$ min (\circ , B), respectively. In presence of either of the IL-2-specific openers Op_1 (\bullet) or Op_2 (\blacktriangledown , both at $25 \mu\text{M}$), neither TNF- α nor IL-1 β mRNA decay is altered. Under the same conditions, an opener designed for TNF- α (Op_T , \star , sequence specified in Table 3) specifically stabilizes the TNF- α mRNA without affecting IL-1 β mRNA levels.

planation for the specificity in mRNA stability regulation. Rather, we found that, in addition to a sequence match, HuR-ARE recognition is dependent on the presentation of NNUUNUUU in single-stranded conformation within the mRNA secondary structure. By combining RNA primary- and secondary-structure properties into a motif accessibility model, we are able to quantitatively understand and predict *in vitro* and cellular, as well as *in vivo* HuR-RNA associations. Previous studies on the NZW mouse strain^[29] have attributed the TNF α -deficient phenotype to a GAU trinucleotide insertion into the TNF α 3'UTR, 5' adjacent to the ARE. It has been shown that the associated down-regulation occurs at the post-transcriptional level, along with reduced complex formation of the mutant mRNA with HuR.^[30] The effect of an insertion outside the ARE core without disruption of HuR binding sites could not be explained mechanistically. If we apply our accessibility model, the decreased HuR binding-site accessibility in mutant versus wild-type TNF α ARE (accessibility ratio 0.59) is in good agreement with the extent of HuR-ARE complex formation (ratio of 0.65^[30]). This provides strong evidence that it is the mutationally altered ARE secondary structure that is responsible for this phenotype.

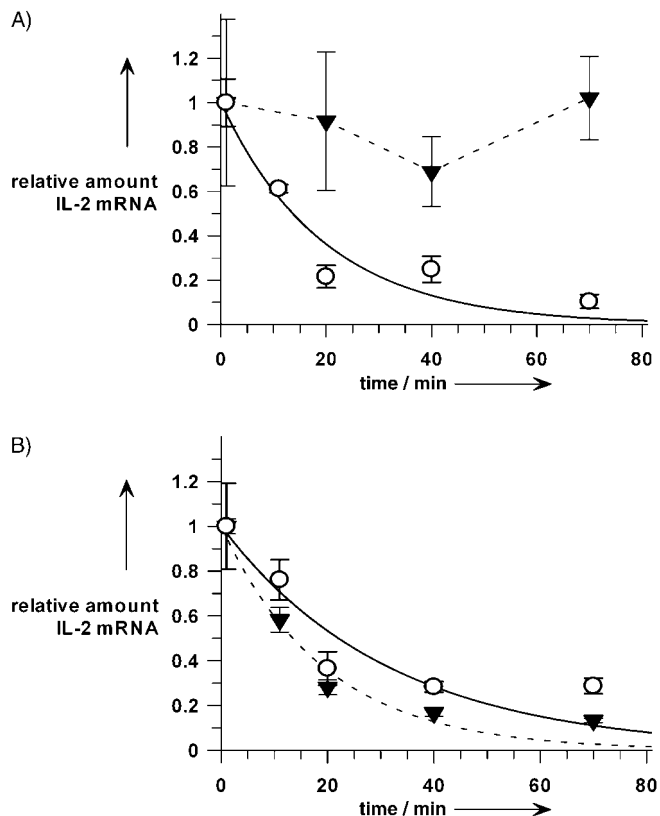


Figure 11. Opener-mediated stabilization can be neutralized with anti-HuR antibody. IL-2 mRNA decay A) in the presence of an HuR-specific antibody, B) control reactions. The stabilization of the IL-2 mRNA induced by opener Op_2 (\circ without opener; \blacktriangledown opener Op_2 at $40 \mu\text{M}$) is neutralized in the presence of a monoclonal anti-HuR antibody.

That the accessibility hypothesis holds in biochemical, cellular biological, and, potentially, also in *in vivo* systems not only supports the validity of the NNUUNUUU consensus and the "all-or-nothing" mechanism. It also suggests the feasibility of using the HuR binding-site presentation as a target for modulation of ARE gene expression in complex biological systems.

mRNA stability manipulation by mRNA openers/closers

With this starting point we proceeded to provide a biochemical and cell biological proof of concept for such a secondary-structure mediated manipulatory on/off switch. Short oligonucleotides were computationally designed to modulate the presentation of the HuR binding motif by hybridizing to their target mRNAs distant or proximal to the HuR binding site. Thereby, these *openers* (*closers*) induce a conformational rearrangement in the mRNA, maximizing (minimizing) the probability of single-stranded NNUUNUUU to promote increased (decreased) stabilization by HuR. Short oligonucleotides or PNAs (peptide nucleic acids) have been used previously to drive the equilibrium between competing secondary structures, for example, in the spliced leader RNA of *Leptomonas collosoma*,^[31] to induce RNA "misfolding"^[32] or to allosterically regulate ribozyme activity.^[33,34] A related concept by Goodchild and co-workers uses facilitator oligonucleotides to enhance ri-

bozyme substrate binding. These facilitators act by coaxial stacking rather than modulating substrate secondary structure.^[35]

We validated our method by designing opener oligonucleotides for IL-2 and TNF α as two ARE-controlled cytokines. Remarkably, predicted opener hybridization sites were confined to "hotspots" within the mRNA, mainly located outside but in proximity to the HuR binding sites. Consequently, the openers target mainly local mRNA secondary structures, for which the prediction is most plausible in a cellular situation. The tested openers were experimentally confirmed to i) enhance HuR-mRNA complex formation in vitro and endogenously as predicted by the algorithm and ii) to specifically induce stabilization of the short-lived ARE mRNA by HuR. While the approximately three- to sevenfold affinity increase induced by the opener demonstrates the functionality of the mechanistic principle, it is not clear why the effect is lower than predicted. One possible explanation might be the limited validity of the assumption that the opener mRNA hybridization reaches saturation, particularly where we used DNA openers. However, the critical parameter for the opener methodology is the functional modulation of the mRNA half-lives in a cellular context. Importantly, this range of affinity increase is sufficient to enhance the stability of IL-2 mRNA in cell lysates from a half-life of 10 to >70 min, close to the endogenous effect in T-cell activation. Also, a similar difference in HuR binding to wild-type versus mutant TNF α mRNA (-40%) leads to a TNF α deficient phenotype of NZW mice.

In the IL-2 mRNA, one of the HuR binding sites individually targeted by two different openers is located outside "the" IL-2 ARE. The functional IL-2 mRNA stabilization by HuR binding to an NNUUNUUU site downstream to the ARE has implications for the understanding of how HuR promotes its stabilizing function. Remarkably, HuR appears to be functional also by binding to sites outside an ARE. No binding site for the negative regulator tristetraprolin^[36] is present in close proximity to the downstream NNUUNUUU site. Consequently, HuR seems not to act by pure displacement of one of its most prominent counterplayers, tristetraprolin.

IL-2 and TNF α were independently stabilized with their respective designed opener oligonucleotides; this leaves the decay of IL-1 β as an additional control, ARE mRNA is unaffected. Thereby, the artificial secondary-structure modulation meets the requirements of high target specificity one would desire for a biochemical and cell biological tool for pathway analyses or other applications in fields like systems biology or drug discovery.

mRNA openers act as a surrogate for CD28 stimulation—a link between functional RNAs and the ARE pathway?

In T-cell activation, the co-stimulatory signal (transduced via CD28) is known to explicitly trigger IL-2 expression by a stabilization of its messenger RNA (e.g. refs. [37,38]). The opener-induced increase in IL-2 mRNA half-life was comparable to the CD28-induced effect previously reported in the literature.^[39] Consequently, the openers mimic the endogenous down-

stream effect of CD28 stimulation in T-cell activation and hence allow specific interference with cellular pathways. This, together with the functional and specific stabilization of individual ARE mRNAs, suggests that such a molecular on/off switch, controlling HuR access in cis might be an elegant and universal solution the cell uses to address specificity in post-transcriptional regulation. A regulatory model based on selective opening/closing of the ARE conformation analogous to the mechanism of the openers (Figure 5) would fulfill all criteria for this regulatory process in a cell: i) a triggerable on/off switch, ii) allowing fast responses and iii) mediating *selective* upregulation of individual messengers in the ubiquitous presence of HuR and target mRNAs.

mRNA openers/closers as tools in systems biology and drug discovery

With the mRNA openers we introduce a method for controlled manipulation of AU-rich element-dependent mRNA levels, potentially complementary to RNAi (see refs. [40–43] for recent reviews). While providing a comparable level of target specificity, the opener (closer) methodology differs from RNAi in several aspects: i) the artificially induced conformational reorganization allows the recognition site of a regulatory factor such as HuR to be both hidden or presented, and can thereby be used to drive the associated regulatory process in both directions. Unlike RNAi or antisense approaches, it therefore not only allows the expression of the target gene to be potentially silenced but also *boosted*, a particular advantage for target validation in drug discovery. ii) The high precision of the computational mRNA opener design reduces the effort that is often required to experimentally assess functional siRNA or antisense hybridization positions. iii) The manipulation is further quantitatively tunable and correlates with the applied opener dose. iv) Functional openers are not dependent on recognition and processing by host cell enzymes (i.e. the Dicer/RISC machinery^[44]). This offers a higher flexibility with respect to the opener nucleic acid length and species, provided that the sequence specificity is not affected. Single-stranded RNA, DNA, or PNA oligonucleotides with virtually any 2'- or backbone modification might be usable; this would allow the metabolic opener stability and its biochemical properties to be adjusted. Also, labeling with fluorescent tags appears feasible. v) In addition, multiple HuR binding sites within one messenger RNA might be individually opened or closed. This would allow the biological role of individual HuR binding sites in the regulation of an mRNA to be successively studied.

While RNAi is applicable to virtually any target gene, the opener methodology remains confined to the set of HuR-controlled genes. However, with an estimated 3000 ARE genes,^[3,45] most of them being tightly controlled and ultimately related to disease-relevant processes, there remains a wide field for potential applications. As this set encompasses functionally diverse genes, distinct pathways in the regulatory network can be studied by interfering at the node of mRNA stability control. As for RNAi, the main issue is the delivery of the opener oligonucleotides into the target cells. It has to be emphasized

that, so far, we have validated the opener effect in human PBMC lysates. Advances in effective but mild transfection methods like optoinjection,^[46] delivery by TAT-peptide chimeras,^[47] or viral vectors for small RNA transcripts promise to make a final proof in vivo attainable.

Given the disease relevance of the majority of HuR–ARE controlled genes, this regulatory system is particularly attractive for therapeutic intervention. Our opener oligonucleotides may serve as tools for making ARE-controlled genes druggable at the level of mRNA conformational rearrangements. Screening for target-specific low-molecular-weight compounds acting as “opener- or closer-mimics” might represent an attractive and suitable concept in drug discovery. With a prototype assay established, virtually any target mRNA within the ARE target platform of up to 3000 genes should become screenable by using a common assay format. In fact, nature exemplifies the potency of small molecules to specifically modulate mRNA secondary structure in the example of riboswitches in the metabolism of Vitamin B12 or glucosamine-6-phosphate.^[48–50]

Altogether, we believe that the mRNA openers/closers will serve as a suitable tool in systems biology and drug discovery research and may encourage future studies addressing a potential link between the ARE pathway and functional RNAs.

Experimental Section

Fluorescently labeled RNA: 5' amino-C6-modified RNA was synthesized on a 394A synthesizer (Applied Biosystems) by using 5'-O-dimethoxytrityl-2'-O-triisopropylloxymethyl-protected β' -cyanoethyl-(*N,N*-diisopropyl)nucleotide phosphoramidites (Glen Research) and adopting published procedures^[51,52] and manufacturer's protocols. The oligoribonucleotides (ORNs) were cleaved from the support, base-, phosphate- and 2'-deprotected and then purified by denaturing polyacrylamide gel electrophoresis by following standard protocols. RNA concentrations were calculated from UV absorption at 260 nm according to Beer's Law, with the exact molar extinction coefficient at 260 nm as determined according to ref. [53]. All ORNs were >99% pure according to analytical reversed-phase high performance liquid chromatography (RP-HPLC) analysis (VYDAC C₁₈ column, 5 μ m, 300 Å, 4.6 \times 250 mm in triethylammonium acetate (0.1 M, pH 7.0) with gradient elution, 0–50% CH₃CN in 45 min, UV detection at 260 nm). 5-Carboxytetramethylrhodamine (TMR, Molecular Probes) was attached to the 5' aminolinker in a standard treatment of the primary amine with a succinimidyl ester-activated fluorophore to form a stable carboxamide. Unreacted dye was hydrolyzed by addition of hydroxylamine-hydrochloride (1.5 M). The labeled RNA was separated from the free dye by gel filtration, purified from unlabeled RNA by RP-HPLC, and the concentration was determined by UV absorption spectroscopy as described above, but with correction for the dye absorption at 260 nm.

3'UTRs were prepared by run-off transcription from dsDNA templates with T7 RNA polymerase (T7 MEGASCRIP in vitro transcription kit, Ambion). The T7 promoter was incorporated into the transcription templates during PCR amplification by using primers encompassing the 3'UTRs of IL-2 and TNF α (IL-2: nt 707–1035, TNF α nt 872–1568, GenBank accession numbers NM_000589 and NM_000594, respectively). The transcript was 3' terminally oxidized with Na(m-)IO₄ and coupled to hydrazide-activated Cy3 (AP Biotech), essentially as described in ref. [54]. The product was subsequently purified by RP-HPLC, as described for synthetic oligoribonucleo-

tides, desalted, and transferred into aqueous solution by gel filtration. A 1:1 labeling stoichiometry was controlled by determination of the Cy3 and RNA concentration by UV/Vis absorption spectroscopy with correction of the dye absorbance at 260 nm.

Recombinant human HuR: The coding sequence for full-length HuR (amino acids 1–326, RefSeq accession: NP_001410) was amplified from cDNA prepared from activated human T-lymphocytes. The product was cloned directionally into the NdeI and SapI sites of the vector pTXB1 (IMPACT™ -CN system, New England Biolabs), allowing C-terminal fusion with an intein-chitin binding domain tag without additional amino acid insertion. The fusion protein was expressed in *E. coli* ER2566 (New England Biolabs) upon induction with IPTG (1 mM, for 6 h at 28 °C). The bacterial cells were lysed by successive freezing/thawing cycles in a buffer of Tris/Cl (tris(hydroxymethyl)aminomethane, 20 mM, pH 8.0), NaCl (800 mM), EDTA (*N,N,N',N'*-ethylenediaminetetraacetic acid, 1 mM) and Pluronic F-127 (0.2% w/v, Molecular Probes). After DNA digestion, the lysates were cleared by ultracentrifugation, and the fusion protein was captured onto chitin agarose beads (New England Biolabs). After extensive washing with lysis buffer, the recombinant protein was recovered by thiol-induced on-column self-splicing of the intein tag with 2-mercaptoethanesulfonic acid (sodium salt, 50 mM) for 12 h at 4 °C.^[55] Any co-eluted intein tag and uncleaved fusion protein were removed from the eluate in a second, subtractive affinity step. The protein was transferred into the storage buffer (Na₂HPO₄/NaH₂PO₄ (25 mM) pH 7.2, NaCl (800 mM), Pluronic F-127 (0.2% w/v)) by gel filtration (DG-10 columns, Bio-Rad), shock-frozen in small aliquots in liquid nitrogen and stored at –80 °C. Under these conditions, full-length HuR was soluble without presence of higher aggregation states (analytical size-exclusion chromatography), and showed the characteristic CD spectra for RRM domains,^[56] data not shown. The protein was >99% pure according to liquid chromatography/electrospray ionization mass spectrometry, RP-HPLC, and SDS-PAGE analysis. N-terminal sequencing revealed a correct N terminus quantitatively missing Met₁. For a precise determination of the concentration, purified HuR was lyophilized, dissolved in guanidinium hydrochloride (6 M), and the concentration was determined by UV spectroscopy according to ref. [57] This solution was used as external standard for the determination of HuR concentrations by RP-HPLC quantification.

2D-FIDA anisotropy HuR–RNA binding assay: The fluorescently labeled RNA was thermally denatured for 2 min at 80 °C in assay buffer (PBS, Pluronic-F-127 (0.1% w/v), MgCl₂ (5 mM)), refolded by cooling to room temperature (–0.13 °C s^{–1}), and diluted to 0.5 nM; this ensured an average of <1 fluorescent particles in the confocal volume in the described setup.^[58] The accurate concentration in each sample was determined based on the particle number derived from a parallel fluorescence correlation spectroscopy evaluation and the size of the confocal volume, as given by the adjustment parameters for the point spread function.^[58] Fluorescently labeled RNA was titrated against increasing concentrations of recombinant HuR (at least 11 titration points). HuR–RNA samples were incubated for at least 15 min at room temperature prior to each measurement.

HuR–RNA complex formation was monitored under true equilibrium conditions by determination of the fluorescence anisotropy with 2D-FIDA. Measurements were performed in 96-well glass-bottom microtiter plates (Whatman) on an EvotecOAI Picko-Screen3 instrument at ambient temperature (constant at 23.5 °C). The Olympus inverted microscope IX70 based instrument was equipped with two fluorescence detectors, a polarization beam splitter in the fluorescence emission path, and an additional linear

polarization filter in the excitation path. A HeNe laser ($\lambda=543$ nm, laser power=495 μ W) was used for fluorescence excitation. The excitation laser light was blocked from the optical detection path by an interference barrier filter with optical density (OD)=5. TMR in assay buffer (at 0.5 nm) was used for the adjustment of the confocal pinhole (70 μ m) and for the determination of the G-factor of the instrument.^[59] The molecular brightness q was extracted from the 2D-FIDA raw data

for each polarization channel by using the FIDA algorithm.^[11,60]

The anisotropy was then calculated as described in ref. [59]. The 2D-FIDA anisotropy signal was averaged from 10 consecutive measurements (10 s each). The G-factor (calculated by using $P_{(\text{true})}$ TMR=0.034) was determined after every 11 measurements.

The anisotropy data were fitted based on the exact algebraic solution of the binding equation describing the average steady-state anisotropy signal r in dependence of the degree of 1:1 complex formation derived from the law of mass action,^[61] to extract the equilibrium dissociation constant $K_{\text{d,app}}$ (nonlinear least-squares regression, GraFit 5.0.3, Erithacus software, London):

$$r = \frac{r_{\text{min}} + (r_{\text{max}} \cdot Q - r_{\text{min}}) \cdot A}{1 - (1 - Q) \cdot A} \quad (4)$$

where:

$$A = \frac{1}{2 \cdot [\text{RNA}_0]} \cdot \left[[\text{RNA}_0] + [\text{HuR}_0] + K_{\text{d,app}} - \sqrt{([\text{RNA}_0] + [\text{HuR}_0] + K_{\text{d,app}})^2 - 4 \cdot [\text{HuR}_0] \cdot [\text{RNA}_0]} \right] \quad (5)$$

where $[\text{RNA}_0]$: total concentration of RNA, $[\text{HuR}_0]$: total concentration of HuR, r_{min} : anisotropy of free RNA, r_{max} : anisotropy of RNA–HuR complex at saturation, r : average anisotropy of the RNA–HuR complex at equilibrium at the given HuR_0 and RNA_0 concentrations; $r = (q_{\parallel} - Gq_{\perp}) / (q_{\parallel} + 2Gq_{\perp})$, q_{\parallel} , q_{\perp} : molecular brightnesses in parallel and perpendicular polarization channels, Q : quenching factor; for 2D-FIDA anisotropy measurements, $Q = q_{\text{tot}(\text{min})} / q_{\text{tot}(\text{max})}$; at $q_{\text{tot}} = q_{\parallel} + 2q_{\perp}$. All presented data are averages of at least three independent experiments.

1D-FIDA HuR–mRNA binding assay: The relative size increase that a fluorescently labeled mRNA or 3'UTR undergoes upon binding the relatively small HuR does not provide a significant detection parameter for the interaction. For this reason, a one-dimensional FIDA assay for HuR binding to 3' terminally Cy3-labeled mRNAs was established. The labeled mRNA was thermally denatured for 2 min at 80 °C in assay buffer (PBS, Pluronic-F-127 (0.1% w/v), MgCl_2 (5 mM)) and refolded by cooling to room temperature (-0.13 °C s⁻¹). Opener or negative-control oligodeoxynucleotides Op₁, Op₂, Op₃, or Neg (MWG Biotech, sequences see Table 3) were added to final concentrations between 0.5 and 100 nM. The final concentration of Cy3-labeled mRNA was 0.5 nM, accurate particle numbers were determined as described for the 2D-FIDA anisotropy measurements.

The labeled mRNA was titrated against increasing concentrations of HuR in the presence and absence of openers or negative-control oligodeoxynucleotides. HuR–mRNA complex formation was monitored under true equilibrium conditions by determination of the molecular brightness with 1D-FIDA.^[62] A HeNe laser ($\lambda=543$ nm, laser power=495 μ W) was used for fluorescence excitation, the optical setup was analogous to the setup for 2D-FIDA anisotropy

measurements, by using only one detection channel and no polarization beam splitters in the optical paths. The molecular brightness was extracted from the 1D-FIDA raw data by using the FIDA algorithm^[62] and averaged from 20 consecutive measurements (10 s each). The molecular brightness data were fitted based on an equation analogous to Equation (4), adapted for fluorescence intensity measurements:

$$q = q_{\text{min}} + \frac{(q_{\text{max}} - q_{\text{min}}) \cdot ([\text{RNA}_0] + [\text{HuR}_0] + K_{\text{d,app}}) - \sqrt{([\text{RNA}_0] + [\text{HuR}_0] + K_{\text{d,app}})^2 - 4 \cdot [\text{RNA}_0] \cdot [\text{HuR}_0]}}{2 \cdot [\text{RNA}_0]} \quad (6)$$

q_{min} : molecular brightness of free RNA, q_{max} : molecular brightness of RNA–HuR complex, q : average molecular brightness for the steady-state equilibrium at the given HuR_0 and RNA_0 concentrations. All presented data are averages of at least three independent experiments.

RNA secondary-structure prediction: RNA secondary structures of minimal free energy were predicted with the program RNAfold, and suboptimal structures with RNAsubopt, both of which are part of the Vienna RNA Package (Version 1.4,^[63] available at www.tbi.univie.ac.at). Illustrations of RNA structures were compiled by using RnaViz.^[64] The distribution of all possible secondary structures σ_i for an RNA molecule of sequence s is called the ensemble, $\varepsilon(s)$. The frequency (thermodynamic probability) of each individual structure σ_i in the ensemble is determined by its stability, that is, its free energy $E(\sigma_i, s)$, and can be calculated by using Boltzmann's law:

$$p(\sigma_i, s) = \frac{e^{E(\sigma_i, s)/kT}}{\sum_{\sigma \in \varepsilon(s)} e^{E(\sigma, s)/kT}} = \frac{e^{E(\sigma_i, s)/kT}}{Q_s} \quad (7)$$

Where Q_s is the partition function of the ensemble.^[65] The probability of a particular structure element A , for example, the probability to find NNUUNUUU in single-stranded conformation is the probability of the ensemble subset containing A and thus a sum of probabilities for all individual structures within this subset (structure probabilities considered to be independent):

$$p(A, s) = \sum_{\sigma_i \in \varepsilon(A, s)} p(\sigma_i, s) = \frac{\sum_{\sigma_i \in \varepsilon(A, s)} e^{E(\sigma_i, s)/kT}}{Q_s} = \frac{Q_{A, s}}{Q_s} \quad (8)$$

Where $\varepsilon(A, s)$ denotes the ensemble subset constrained to structures containing A , and $Q_{A, s}$ is the respective partition function.

For a correlation with affinity data, only the discrimination *accessible* and *inaccessible* will be of interest. Equation (8) is valid for structure elements with single occurrence in a molecule. As an element of interest may occur repeatedly and may overlap, the definition of p is extended to the probability of structures containing *at least one* element A . A computation via the probability of its complement is not possible due to limitations for constrained folding. As the probabilities of jointly occurring substructures are not independent, the sum of the individual probabilities has to be corrected:

$$p(A_1 \cup A_2 \cup \dots \cup A_{n-1} \cup A_n) = \sum_{i < n} \frac{Q_{A_i, s}}{Q_s} - \sum_{i < j < n} \frac{Q_{A_i, A_j, s}}{Q_s} + \sum_{i < j < k < n} \frac{Q_{A_i, A_j, A_k, s}}{Q_s} - \sum_{i < j < k < l < n} \frac{Q_{A_i, A_j, A_k, A_l, s}}{Q_s} \quad (9)$$

Where $Q_{A_1, A_2, \dots, A_n, s}$ denotes the partition function of the ensemble constrained to structures containing the j^{th} , j^{th} , ..., n^{th} occurrence of element A . To minimize numerical errors, the probabilities are cal-

culated with the ensemble free energies W of $\varepsilon(s)$ and $\varepsilon(A,s)$ ($W = -RT \ln Q$); this results in $p(A,s) = \exp((W_{\varepsilon(s)} - W_{\varepsilon(A,s)})R^{-1}T^{-1})$. Ensemble free energies are computed by using the Perl module of RNA_{FOLD}. The calculation of Q_s is straightforward; $Q_{A,s}$ is calculated by constraining the subsequence corresponding to the i^{th} occurrence of A to the structure element A .

Prediction of opener oligonucleotides: We define openers (closers) as short oligonucleotide sequences reverse complementary to their target mRNA that, upon hybridization, change the secondary structure of their target so that the HuR binding-site accessibility is maximized (minimized). For simplicity of calculation we assume: i) all opener nucleotides form base pairs with their respective reverse complement in the target mRNA exclusively, that is, no sub-optimal interactions between opener and target are considered, ii) the equilibrium between opener-bound target and free target is neglected, that is, all target mRNA molecules are hybridized to the opener, iii) no energy contributions from the opener–target hybridization are included in the prediction of the opener-bound target mRNA's secondary structure. The effect of the opener is solely modeled by excluding the opener-bound nucleotides in the target mRNA from internal base pairing.

The binding-site accessibility of an mRNA with an opener hybridized at mRNA sequence position n $p(ssNNUUNUUU|opener_n)$ was calculated for all $(length_{\text{target}} - length_{\text{opener}} + 1)$ possible opener positions by using the above-described algorithm, additionally constraining the opener-bound nucleotides in the target mRNA to be single stranded. The opener length was arbitrarily set to 20 nucleotides. Opener positions at which the binding-site accessibility was locally maximized were finally selected for experimental testing. The described approach can be generalized for the prediction of reverse complementary oligonucleotides that favor any RNA secondary-structure element in the ensemble.

Preparation and stimulation of cells: Human peripheral blood monocyte cells (PBMC) were isolated from heparinized blood by Ficoll-Hypaque centrifugation, washed with PBS containing bovine serum albumin (BSA, 15% w/v), resuspended at $2 \times 10^6 \text{ mL}^{-1}$ in RPMI1640 (Gibco/BRL) supplemented with heat-inactivated fetal calf serum (10% v/v), L-glutamine (2 mM), streptomycin ($100 \mu\text{g mL}^{-1}$), and penicillin (100 u mL^{-1}), and incubated in a 37°C CO_2 incubator. PBMC were stimulated for 4 h with phorbol 12-myristate 13-acetate (PMA, 25 ng mL^{-1} , Sigma–Aldrich) and anti-CD3 mAb ($1 \mu\text{g mL}^{-1}$, Pharmingen) in the absence and presence of anti-CD28 mAb ($1 \mu\text{g mL}^{-1}$, Pharmingen).

Co-immunoprecipitation of HuR–mRNA complexes: For each immunoprecipitation, 5×10^6 nonstimulated cells were washed with PBS/BSA and lysed at 4°C in hypotonic buffer (100 μL , Tris/Cl (10 mM) pH 7.5, NaCl (10 mM), EDTA (10 mM), protease inhibitor (Complete Mini EDTA-free Protease Inhibitor Cocktail, Roche; 3 tablets per 50 mL lysis buffer) and Nonidet-P-40 (0.5% v/v)). RNasin (0.4 u mL^{-1} , Promega) and SupersalN (0.2 u mL^{-1} , Ambion) were added to inhibit unspecific RNA degradation. The lysates were centrifuged at 4°C for 4 min at $15000 \times g$ to pellet nuclei. The cleared lysates were incubated for 5 min with anti-HuR mAb (5 $\mu\text{g mL}^{-1}$, 19F12, Molecular Probes) at 4°C in the presence and absence of opener or negative-control oligonucleotides Op_1 , Op_2 , or Neg (at 2.5 or 10 μM). After addition of biotinylated anti-mouse IgG mAb (10 $\mu\text{g mL}^{-1}$, Amersham Pharmacia), the immune complexes were captured on streptavidin sepharose beads (Amersham Pharmacia). The beads were washed thoroughly with lysis buffer. HuR and the complexed mRNA were eluted under acidic conditions (Glycin/HCl (50 mM, pH 2.5), NaCl (50 mM), prewarmed to 95°C). The eluates were passed by centrifugation through BioSpin gel filtration col-

umns (BioRad), pre-equilibrated with H_2O . Co-precipitated RNA was quantified by real-time RT-PCR.

mRNA decay: 5×10^6 stimulated PBMC were lysed in lysis buffer (250 μL) as described above, in the presence or absence of opener or negative-control oligonucleotides Op_1 , Op_2 , Op_3 , Neg (at 10, 25, or 40 μM). For neutralization studies, a monoclonal antibody specifically recognizing HuR (19F12, Molecular Probes) was added to the lysates to a final concentration of $30 \mu\text{g mL}^{-1}$. mRNA degradation was initiated in the cleared lysates by addition of MgCl_2 (net concentration of 5 mM free Mg^{2+}). The degradation reaction proceeded at room temperature and was stopped after various time points between 2 and 70 min incubation (50 μL aliquots for each time point) by addition of EDTA and guanidinium isothiocyanate-containing buffer (Qiagen). RNA was isolated by using the RNeasy Miniprep RNA isolation kit (Qiagen) according to the manufacturer's protocol, with DNase I treatment for the elimination of residual DNA.

Quantitative real-time RT-PCR: RNA was reverse transcribed to cDNA with the TaqMan RT-PCR reagents (Applied Biosystems) and random hexamers for priming by following standard protocols. Control reactions for genomic DNA contamination were performed without addition of reverse transcriptase. Quantitative RT-PCR was performed with SYBR Green detection on an ABI7700 instrument (Applied Biosystems) with the following primers: IL-2 mRNA: forward: 5'-TCACCAGGATGCTCACATTTAAGTT-3'; reverse: 5'-GGAGTTT-GAGTCTTCTTAGACACTGA-3'; TNF α mRNA: forward: 5'-AGGCGGTGCTGTTCCTC-3'; reverse: 5'-GTTCGAGAAGATGATCT-GACTGCC-3'; IL-1 β mRNA: forward: 5'-GTACCTGAGCTCGCCAGTGA-3'; reverse: 5'-TCGGAGATTCGTAGCTGGATG-3' (Primers were a gift from F. Kalthoff, Novartis Institute for Biomedical Research Vienna). EF-1 α was used as endogenous control (primers: forward 5'-TTTGAGACCAGCAAGTACTATGTGACT-3', reverse 5'-TCAGCCTGAGATGTCCCTGTAA-3'). The $\Delta\Delta\text{Ct}$ method was used for relative quantification of IL-2 mRNA levels (as described in, for example, ref. [66]) with in vitro transcribed IL-2 mRNA for calibration. All presented data are averages of at least five identical independent samples and representative of at least two independent experiments with cells from independent donors.

Acknowledgements

The authors are grateful to Siegfried Höfner for contribution to the Table of Contents figure, to Peter Stadler, Ivo Hofacker, Kurt Grünberger, Christoph Flamm, Frank Kalthoff, Marcus Rudin, and Ivan Lindley for helpful discussions and to Manuel Peitsch, René Amstutz, and Jan deVries for continuous support. This work was partly supported by the Austrian Academy of Sciences (DOC 11/2000).

Keywords: AU-rich elements · functional RNAs · HuR · RNA recognition · RNA structures · systems biology

- [1] C. M. Brennan, J. A. Steitz, *Cell. Mol. Life Sci.* **2001**, *58*, 266–277.
- [2] A. Bevilacqua, M. C. Ceriani, S. Capaccioli, A. Nicolini, *J. Cell. Physiol.* **2003**, *195*, 356–372.
- [3] T. Bakheet, M. Frevel, B. R. G. Williams, W. Greer, K. S. A. Khabar, *Nucleic Acids Res.* **2001**, *29*, 246–254.
- [4] N. S. Levy, S. Chung, H. Furneaux, A. P. Levy, *J. Biol. Chem.* **1998**, *273*, 6417–6423.
- [5] J. L. E. Dean, R. Wait, K. R. Mahtani, G. Sully, A. Clark, J. Saklatvala, *Mol. Cell. Biol.* **2001**, *21*, 721–730.

- [6] W. Wang, H. Furneaux, H. Cheng, C. Caldwell, D. Hutter, Y. Liu, N. Holbrook, M. Gorospe, *Mol. Cell. Biol.* **2000**, *20*, 760–769.
- [7] K. Mazan-Mamczarz, S. Galbán, I. López de Silanes, J. L. Martindale, U. Atasoy, J. D. Keene, M. Gorospe, *Proc. Natl. Acad. Sci. USA* **2003**, *100*, 8354–8359.
- [8] F. Rodriguez-Pascal, M. Hausding, I. Ihrig-Biedert, H. Furneaux, A. P. Levy, U. Förstermann, H. Kleinert, *J. Biol. Chem.* **2000**, *275*, 26040–26049.
- [9] W. Wang, C. Caldwell, S. Lon, H. Furneaux, M. Gorospe, *EMBO J.* **2000**, *19*, 2340–2350.
- [10] C. Y. Chen, N. Xu, A. B. Shyu, *Mol. Cell. Biol.* **2002**, *22*, 7268–7278.
- [11] P. Kask, K. Palo, D. Ullmann, K. Gall, *Proc. Natl. Acad. Sci. USA* **1999**, *96*, 13756–13761.
- [12] I. López de Silanes, J. Fan, X. Yang, A. B. Zonderman, O. Potapova, E. S. Pizer, M. Gorospe, *Oncogene* **2003**, *22*, 7146–7154.
- [13] V. E. Myer, X. C. Fan, J. A. Steitz, *EMBO J.* **1997**, *16*, 2130–2139.
- [14] B. B. Yeap, D. C. Voon, J. P. Vivian, R. K. McCulloch, A. M. Thomson, K. M. Giles, M. F. Czyzyk-Krzeska, H. Furneaux, M. C. J. Wilce, J. A. Wilce, P. J. Leedman, *J. Biol. Chem.* **2002**, *277*, 27183–27192.
- [15] X. Wang, T. M. Tanaka Hall, *Nat. Struct. Biol.* **2001**, *8*, 141–145.
- [16] N. Xu, C. Y. Chen, A. B. Shyu, *Mol. Cell. Biol.* **1997**, *17*, 4611–4621.
- [17] N. Handa, O. Nureki, K. Kurimoto, I. Kim, H. Sakamoto, Y. Shimura, Y. Muto, S. Yokoyama, *Nature* **1999**, *398*, 579–585.
- [18] G. Varani, K. Nagai, *Annu. Rev. Biophys. Biomol. Struct.* **1998**, *27*, 407–445.
- [19] Z. Liu, I. Luyten, M. J. Bottomley, A. C. Messias, S. Houngrinou-Molanggo, R. Sprangers, K. Zanier, A. Kramer, M. Sattler, *Science* **2001**, *294*, 1098–1102.
- [20] D. Cooper, I. Dunsmore, J. Gower, P. Jones, I. Lloyd, E. O'Connell, A. Smith, G. Tunnicliffe-Wilson, D. Warren, J. Whittaker in *Statistics Part B, Vol. VI* (Eds.: E. Lloyd), Wiley, New York, **1984**, pp. 689–725.
- [21] A. Raghavan, R. L. Robison, J. McNabb, C. R. Miller, D. A. Williams, P. R. Bohjanen, *J. Biol. Chem.* **2001**, *276*, 47958–47965.
- [22] L. P. Ford, J. Watson, J. D. Keene, J. Wilusz, *Genes Dev.* **1999**, *13*, 188–201.
- [23] H. Tran, F. Maurer, Y. Nagamine, *Mol. Cell. Biol.* **2003**, *23*, 7177–7188.
- [24] W.-J. Ma, S. Chung, H. Furneaux, *Nucleic Acids Res.* **1997**, *25*, 3564–3569.
- [25] G. Wein, M. Rossler, R. Klug, T. Herget, *Eur. J. Biochem.* **2003**, *270*, 350–365.
- [26] Y. Seko, H. Azmi, R. Fariss, J. A. Ragheb, *J. Biol. Chem.* **2004**, *279*, 33359–33367.
- [27] Z. Zhao, F.-C. Chang, H. Furneaux, *Nucleic Acids Res.* **2000**, *28*, 2695–2701.
- [28] M. Kullmann, U. Gopfert, B. Siewe, L. Hengst, *Genes Dev.* **2002**, *16*, 3087–3099.
- [29] C. O. Jacob, S. K. Lee, G. Strassmann, *J. Immunol.* **1996**, *156*, 3043–3050.
- [30] S. Di Marco, Z. Hel, C. Lachance, H. Furneaux, D. Radzioch, *Nucleic Acids Res.* **2001**, *29*, 863–871.
- [31] K. A. LeCuyer, D. M. Crothers, *Proc. Natl. Acad. Sci. USA* **1994**, *91*, 3373–3377.
- [32] J. L. Childs, M. D. Disney, D. H. Turner, *Proc. Natl. Acad. Sci. USA* **2002**, *99*, 11091–11096.
- [33] Y. Komatsu, *Biol. Pharm. Bull.* **2004**, *27*, 457–462.
- [34] Y. Komatsu, S. Yamashita, N. Kazama, K. Nobuoka, E. Ohtsuka, *J. Mol. Biol.* **2000**, *299*, 1231–1243.
- [35] T. A. Perkins, D. E. Wolf, J. Goodchild, *Biochemistry* **1996**, *35*, 16370–16377.
- [36] P. J. Blackshear, W. S. Lai, E. A. Kennington, G. Brewer, G. M. Wilson, X. Guan, P. Zhou, *J. Biol. Chem.* **2003**, *278*, 19947–19955.
- [37] J. D. Powell, J. A. Ragheb, S. Kitagawa-Sakakida, R. H. Schwartz, *Immunol. Rev.* **1998**, *165*, 287–300.
- [38] J. Shim, H. Lim, R. Yates, M. Karin, *Mol. Cell* **2002**, *10*, 1331–1344.
- [39] A. Raghavan, R. L. Ogilvie, C. Reilly, M. L. Abelson, S. Raghavan, J. Vas-dewani, M. Krathwohl, P. R. Bohjanen, *Nucleic Acids Res.* **2002**, *30*, 5529–5538.
- [40] P. D. Zamore, T. Tuschl, P. A. Sharp, D. P. Bartel, *Cell* **2000**, *101*, 25–33.
- [41] S. M. Elbashir, W. Lendeckel, T. Tuschl, *Genes Dev.* **2001**, *15*, 188–200.
- [42] A. M. Denli, G. J. Hannon, *Trends Biochem. Sci.* **2003**, *28*, 196–201.
- [43] N. Agrawal, P. V. Dasaradhi, A. Mohammed, P. Malhotra, R. K. Bhatnagar, S. K. Mukherjee, *Microbiol. Mol. Biol. Rev.* **2003**, *67*, 657–685.
- [44] M. A. Carmell, G. J. Hannon, *Nat. Struct. Mol. Biol.* **2004**, *11*, 214–218.
- [45] T. Bakheet, B. R. Williams, K. S. Khabar, *Nucleic Acids Res.* **2003**, *31*, 421–423.
- [46] M. R. Koller, E. G. Hanania, G. Sasaki, B. O. Palsson, <http://www.cyntellect.com>
- [47] N. Nitin, P. J. Santangelo, G. Kim, S. Nie, G. Bao, *Nucleic Acids Res.* **2004**, *32*, e58.
- [48] M. Mandal, B. Boese, J. E. Barrick, W. C. Winkler, R. R. Breaker, *Cell* **2003**, *113*, 577–586.
- [49] W. C. Winkler, R. R. Breaker, *ChemBioChem* **2003**, *4*, 1024–1032.
- [50] W. C. Winkler, A. Nahvi, A. Roth, J. A. Collins, R. R. Breaker, *Nature* **2004**, *428*, 281–286.
- [51] C. Chaix, A. M. Duplax, D. Gasparutto, D. Molko, R. Teoule, *Nucleic Acids Symp. Ser.* **1989**, 45–46.
- [52] S. A. Scaringe, C. Francklyn, N. Usman, *Nucleic Acids Res.* **1990**, *18*, 5433–5441.
- [53] D. M. Gray, S. H. Hung, K. H. Johnson, *Methods Enzymol.* **1995**, *246*, 19–34.
- [54] P. Z. Qin, A. M. Pyle, *Methods* **1999**, *18*, 60–70.
- [55] S. Chong, F. B. Perler, *Intein-Mediated Protein Purification in Methods and Tools in Biosciences and Medicine*, (Ed.: M. Blot), Birkhauser, Basel, **2003**, pp. 173–193.
- [56] X. Manival, L. Ghisolfi-Nieto, G. Joseph, P. Bouvet, M. Erard, *Nucleic Acids Res.* **2001**, *29*, 2223–2233.
- [57] S. C. Gill, P. H. von Hippel, *Anal. Biochem.* **1989**, *182*, 319–326.
- [58] Evotec BioSystems AG, *2D-FIDA-Quick-Guide*, Evotec Biosystems, Hamburg, **2001**, pp. 10.
- [59] J. R. Lakowicz, *Principles of Fluorescence Spectroscopy*, Plenum, New York, **1999**, pp. 291–319.
- [60] P. Kask, K. Palo, N. Fay, L. Brand, U. Mets, D. Ullmann, J. Jungmann, J. Pschorr, K. Gall, *Biophys. J.* **2000**, *78*, 1703–1713.
- [61] T. J. Daly, R. C. Doten, J. R. Rusche, M. Auer, *J. Mol. Biol.* **1995**, *253*, 243–258.
- [62] P. Kask, K. Palo, D. Ullmann, K. Gall, *Proc. Natl. Acad. Sci. USA* **1999**, *96*, 13756–13761.
- [63] I. L. Hofacker, W. Fontana, P. F. Stadler, S. Bonhoeffer, M. Tacker, P. Schuster, *Monatsh. Chem.* **1994**, *125*, 167–188.
- [64] P. De Rijk, J. Wuyts, R. De Wachter, *Bioinformatics* **2003**, *19*, 299–300.
- [65] J. S. McCaskill, *Biopolymers* **1990**, *29*, 1105–1119.
- [66] Applied Biosystems, **2000**, ABI PRISM 7700 Sequence Detection System, Users Manual, P/N904989B.
- [67] D. J. Adams, D. J. Beveridge, L. van der Weyden, H. Mangs, P. J. Leedman, B. J. Morris, *J. Biol. Chem.* **2003**, *278*, 44894–44903.
- [68] L. B. Nabors, G. Y. Gillespie, L. Harkins, P. H. King, *Cancer Res.* **2001**, *61*, 2154–2161.
- [69] U. Atasoy, S. L. Curry, I. López de Silanes, A. B. Shyu, V. Casolaro, M. Gorospe, C. Stellato, *J. Immunol.* **2003**, *171*, 4369–4378.
- [70] I. Raineri, D. Wegmueller, B. Gross, U. Certa, C. Moroni, *Nucleic Acids Res.* **2004**, *32*, 1279–1288.
- [71] S. Esnault, J. S. Malter, *J. Immunol.* **2003**, *171*, 6780–6787.
- [72] U. Atasoy, J. Watson, D. Patel, J. D. Keene, *J. Cell Sci.* **1998**, *111*, 3145–3156.
- [73] R. Manjithaya, R. R. Dighe, *Biol. Reprod.* **2004**, in press.
- [74] C. Abraham, J. Miller, *J. Immunol.* **2001**, *167*, 5193–5201.
- [75] W.-J. Ma, S. Cheng, C. Campbell, A. Wright, H. Furneaux, *J. Biol. Chem.* **1996**, *271*, 8144–8151.
- [76] X. F. Ming, G. Stoecklin, M. Lu, R. Looser, C. Moroni, *Mol. Cell. Biol.* **2001**, *21*, 5778–5789.
- [77] R. Winzen, G. Gowrishankar, F. Bollig, N. Redich, K. Resch, H. Holtmann, *Mol. Cell. Biol.* **2004**, *24*, 4835–4847.
- [78] L. B. Nabors, E. Suswam, Y. Huang, X. Yang, M. J. Johnson, P. H. King, *Cancer Res.* **2003**, *63*, 4181–4187.
- [79] A. Figueroa, A. Cuadrado, J. Fan, U. Atasoy, G. E. Muscat, P. Muñoz-Canoves, M. Gorospe, A. Muñoz, *Mol. Cell. Biol.* **2003**, *23*, 4991–5004.
- [80] K. van der Giessen, S. DiMarco, E. Clair, I. Gallouzi, *J. Biol. Chem.* **2003**, *278*, 47119–47128.
- [81] J. Haeussler, J. Haeusler, A. M. Striebel, G. Assum, W. Vogel, H. Furneaux, W. Krone, *Biochem. Biophys. Res. Commun.* **2000**, *267*, 726–732.

- [82] P. Briata, C. Ilengo, G. Corte, C. Moroni, M. G. Rosenfeld, C. Y. Chen, R. Gherzi, *Mol. Cell* **2003**, *12*, 1201–1211.
- [83] M. R. McMullen, E. Cocuzzi, M. Hatzoglou, L. E. Nagy, *J. Biol. Chem.* **2003**, *278*, 38333–38341.
- [84] Z. Hel, S. DiMarco, D. Radzioch, *Nucl. Acids. Res.* **1998**, *26*, 2803–2812.
- [85] K. Sakai, Y. Kitagawa, G. Hirose, *FEBS Lett.* **1999**, *446*, 157–162.
- [86] I. Goldberg-Cohen, H. Furneaux, A. P. Levy, *J. Biol. Chem.* **2002**, *277*, 13635–13640.
- [87] A. P. Levy, *Trends Cardiovasc. Med.* **1998**, *8*, 246–250.
- [88] K. Tang, E. C. Breen, P. D. Wagner, *Am. J. Physiol. Heart Circ. Physiol.* **2002**, *283*, H1497–H1504.
- [89] D. A. Dixon, N. D. Tolley, P. H. King, L. B. Nabors, T. M. McIntyre, G. A. Zimmerman, S. M. Prescott, *J. Clin. Invest.* **2001**, *108*, 1657–1665.
- [90] W. Wang, J. Fan, X. Yang, S. Furer-Galban, I. López de Silanes, C. von Kobbe, J. Guo, S. N. Georas, F. Fougelle, D. G. Hardie, D. Carling, M. Gorospe, *Mol. Cell. Biol.* **2002**, *22*, 3425–3436.
- [91] J. Hauber, A. T. Prechtel, US 2002/165 186 A1.
- [92] K. M. Giles, J. M. Daly, D. J. Beveridge, A. M. Thomson, D. C. Voon, H. M. Furneaux, J. A. Jazayeri, P. J. Leedman, *J. Biol. Chem.* **2003**, *278*, 2937–2946.
- [93] I. López de Silanes, M. Zhan, A. Lal, X. Yang, M. Gorospe, *Proc. Natl. Acad. Sci. USA* **2004**, *101*, 2987–2992.
- [94] S. S.-Y. Peng, C.-Y. A. Chen, N. Xu, A.-B. Shyu, *EMBO J.* **1998**, *17*, 3461–3470.
- [95] W. Wang, X. Yang, V. J. Cristofalo, N. J. Holbrook, M. Gorospe, *Mol. Cell. Biol.* **2001**, *21*, 5889–5898.
- [96] I. Lafon, F. Carballes, G. Brewer, M. Poirer, D. Morello, *Oncogene* **1998**, *16*, 3413–3421.
- [97] A. Gouble, D. Morello, *Oncogene* **2000**, *19*, 5377–5384.
- [98] C. F. Manohar, M. L. Short, A. Nguyen, N. N. Nguyen, D. Chagnovich, Q. Yang, S. L. Cohn, *J. Biol. Chem.* **2002**, *277*, 1967–1973.
- [99] S. Galban, J. L. Martindale, K. Mazan-Mamczarz, I. López de Silanes, I. J. Fan, W. Wang, J. Decker, M. Gorospe, *Mol. Cell. Biol.* **2003**, *23*, 7083–7095.
- [100] E.-S. Akool, H. Kleinert, F. M. Hamada, M. H. Abdelwahab, U. Forstermann, J. Pfeilschifter, W. Eberhardt, *Mol. Cell. Biol.* **2003**, *23*, 4901–4916.
- [101] A. Huwiler, E.-S. Akool, A. Aschrafi, F. M. Hamada, J. Pfeilschifter, W. Eberhardt, *J. Biol. Chem.* **2003**, *278*, 51758–51769.
- [102] S. J. Cok, S. J. Acton, A. E. Sexton, A. R. Morrison, *J. Biol. Chem.* **2004**, *279*, 8196–8205.
- [103] K. Subbaramaiah, T. P. Marmao, D. A. Dixon, A. J. Dannenberg, *J. Biol. Chem.* **2003**, *278*, 37637–37647.
- [104] S. Sengupta, B. C. Jang, M. T. Wu, J. H. Paik, H. Furneaux, T. Hla, *J. Biol. Chem.* **2003**, *278*, 25227–25233.
- [105] C. Denkert, W. Weichert, S. Pest, I. Koch, D. Licht, M. Kobel, A. Reles, J. Sehouli, M. Dietel, S. Hauptmann, *Cancer Res.* **2004**, *64*, 189–195.
- [106] F. Maurer, M. Tierney, R. L. Medcalf, *Nucleic Acids Res.* **1999**, *27*, 1664–1673.
- [107] B. C. Blaxall, A. C. Pellett, S. C. Wu, A. Pende, J. D. Port, *J. Biol. Chem.* **2000**, *275*, 4290–4297.
- [108] B. C. Blaxall, J. D. Port, *Methods Mol. Biol.* **2000**, *126*, 453–465.
- [109] J. A. Wilce, P. J. Leedman, M. C. Wilce, *IUBMB Life* **2002**, *54*, 345–349.
- [110] S. Yasuda, S. Wada, Y. Arai, M. Kogawa, F. Kayama, S. Katayama, *Endocrinology* **2004**, *145*, 1730–1738.
- [111] S. Chung, M. Eckrich, N. Perrone-Bizzozero, D. T. Kohn, H. Furneaux, *J. Biol. Chem.* **1997**, *272*, 6593–6598.
- [112] R. G. Jain, L. G. Andrews, K. M. McGowan, F. Gao, J. D. Keene, P. P. Pekala, *Nucleic Acids Symp. Ser.* **1995**, 209–211.
- [113] P. Loflin, J. E. Lever, *FEBS Lett.* **2001**, *509*, 267–271.
- [114] K. Sakai, Y. Kitagawa, M. Saiki, S. Saiki, G. Hirose, *Mol. Immunol.* **2003**, *39*, 879–883.
- [115] I. Yaman, J. Fernandez, H. Liu, M. Caprara, A. A. Komar, A. E. Koromilas, L. Zhou, M. D. Snider, D. Scheuner, R. J. Kaufman, M. Hatzoglou, *Cell* **2003**, *113*, 519–531.
- [116] No binding refers to the detection limit of our assay: the complex formation becomes undetectable at <3 sd change in the anisotropy signal at the maximum HuR concentration of 5–10 μM in the assay (solubility limit of full length HuR). This corresponds to a K_d detection limit of approximately >100 μM. In relation to the fundamental K_d of 1 nM, we henceforth refer to this >100 000-fold difference in the affinity as “all-or-nothing”).

Received: June 30, 2004